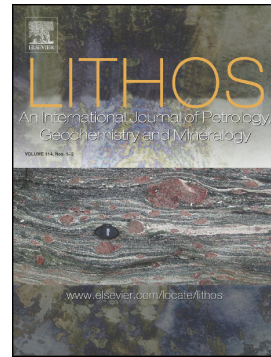


Accepted Manuscript

Late Eocene granites in the Central Sakhalin Island (Russian Far East) and its implication for evolution of the Sakhalin-Hokkaido orogenic belt

Pan Zhao, Igor Alexandrov, Bor-ming Jahn, Jia-Ping Liao, Vitaly Ivin



PII: S0024-4937(18)30464-X

DOI: <https://doi.org/10.1016/j.lithos.2018.12.002>

Reference: LITHOS 4893

To appear in: *LITHOS*

Received date: 10 July 2018

Accepted date: 3 December 2018

Please cite this article as: Pan Zhao, Igor Alexandrov, Bor-ming Jahn, Jia-Ping Liao, Vitaly Ivin , Late Eocene granites in the Central Sakhalin Island (Russian Far East) and its implication for evolution of the Sakhalin-Hokkaido orogenic belt. *Lithos* (2018), <https://doi.org/10.1016/j.lithos.2018.12.002>

This is a PDF file of an unedited manuscript that has been accepted for publication. As a service to our customers we are providing this early version of the manuscript. The manuscript will undergo copyediting, typesetting, and review of the resulting proof before it is published in its final form. Please note that during the production process errors may be discovered which could affect the content, and all legal disclaimers that apply to the journal pertain.

Late Eocene granites in the central Sakhalin Island (Russian Far East) and its implication for evolution of the Sakhalin-Hokkaido orogenic belt

Pan Zhao^{1,2,*} pan.zhao@ifg.uni-tuebingen.de, Igor Alexandrov^{3,4}, Bor-ming Jahn¹, Jia-Ping Liao¹, and Vitaly Ivin³

¹Department of Geosciences, National Taiwan University, Taipei, 10617, Taiwan

²Fachbereich Geowissenschaften, Universität Tübingen, Tübingen, 72076, Germany

³Far East Geological Institute, Far Eastern Branch of the Russian Academy of Sciences, Vladivostok, Russia

⁴School of Engineering, Far Eastern Federal University, Vladivostok, 690950, Russia

*Corresponding author.

¹ Deceased

Abstract:

The Sakhalin-Hokkaido orogenic belt along the western margin of the Okhotsk Sea is an important early Cenozoic accretionary orogen related to subduction of the Paleo-Pacific oceanic plate. In order to study the Eocene evolution of this accretionary orogen and related magmatism, we carried out zircon U-Pb dating, whole-rock elemental and Sr-Nd isotopic analyses on the Langeri and Val'za granitic plutons that intruded the East Sakhalin accretionary complex in the central Sakhalin Island. Zircon U-Pb dating results revealed that the Langeri and Val'za plutons were emplaced in the late Eocene at 38-36 Ma. Whole-rock elemental data indicate that granitoids are mainly peraluminous S-type with subordinate I-type granites, and all granitic samples show arc-like geochemical affinity. Whole-rock Sr-Nd isotopic results show consistent low initial $^{87}\text{Sr}/^{86}\text{Sr}$ ratios (0.7042 to 0.7049), positive $\varepsilon_{\text{Nd}}(t)$ values (+1.7 to +3.1) and young Nd two-stage model ages (611 to 717 Ma). Elemental and isotopic data reveal that granitic rocks of the Langeri and Val'za plutons were generated from remelting of metasediments and amphibolites in the accretionary complex. From comprehensive analyses of regional tectonics, we concluded that the late Eocene granitic rocks were generated in a syn-collisional tectonic setting, marking the timing for formation of the Sakhalin-Hokkaido orogenic belt. The middle-late Eocene welding of the Okhotsk Sea Plate and the Eurasia Plate is the most plausible mechanism that caused crustal thickening beneath the Sakhalin Island, and anatexis of metasediments and oceanic crustal materials in the lower crust might be responsible for the formation of late Eocene granitic rocks. Considering the Eocene tectonic events in NE Asia, late Paleocene to early Eocene subduction of the Kula-Pacific ridge beneath the Hokkaido Island and Eocene initial rift of pull-apart basins

along strike-slip fault system in the Hokkaido and Sakhalin Islands may also contribute to the emplacement of Eocene magmatism in the Sakhalin-Hokkaido orogenic belt.

Keywords: Sakhalin-Hokkaido orogenic belt; late Eocene; peraluminous granite; geochemistry; syn-collisional setting

1. Introduction

The Sakhalin-Hokkaido orogenic belt along the western margin of the Okhotsk Sea belongs to the northern part of the Western Pacific Orogenic Belt or the Nipponides (Fig. 1a; Sengör and Natal'in, 1996). Prior to the opening of Japan Sea and Tatar Strait, accretionary terranes in the Sikhote-Alin region, Sakhalin and Japanese Islands represented the northeastern margin of the Asian Continent. The successive accretion of these terranes started from the Jurassic in the western Sikhote-Alin and southwestern Japan and ceased around the early Paleogene in the eastern Sakhalin and Hokkaido Islands (Fig. 1b; Khanchuk, 2001). The Sikhote-Alin orogenic belt is constituted by terranes of accretionary prisms, turbidite basins and island arc systems in the age of Jurassic to late Cretaceous (Fig. 1b; Khanchuk, 2001; Khanchuk et al., 2016). These accretionary terranes are intruded by the Cretaceous to earliest Paleogene granitoids and overlain by coeval volcanic rocks (Table 1; Kruk et al., 2014; Jahn et al., 2015; Khanchuk et al., 2016; Grebennikov et al., 2016; Zhao et al., 2017a; Wu et al., 2017), constituting the East Sikhote-Alin Volcanic-Plutonic Belt (Khanchuk, 2001), which extends northeastward along the continental margin of northeast Asia (Zhao et al., 2017a). From reviewing the late Cretaceous-Paleogene magmatism along the northeastern margin of Asia, it can be concluded that the Cretaceous-early Paleocene magmatic rocks are mainly calc-alkaline I-type and subduction-related (Akinin and Miller, 2011; Jahn et al., 2015; Zhao et al., 2017a; Martynov et al., 2017), whereas the late Paleocene-Eocene magmatic rocks are mainly collision-related, extension-related or transtension-related (Luchitskaya and Soloviev, 2012; Leonova et al., 2015; Filatova, 2015; Grebennikov et al., 2016; Martynov et al., 2017; Liao et al., 2018). The Sakhalin Island is mainly

composed of the late Early Cretaceous (Aptian) to early Paleogene fore-arc turbidite basin and coeval accretionary complex along the eastern margin of the Sikhote-Alin orogenic belt due to subduction of the Paleo-Pacific oceanic plate (Khanchuk, 2001). The Sakhalin Island has been tectonically correlated with the Hokkaido Island in northeastern Japan as evidenced by geological, paleontological, petrological, and magnetostratigraphic similarities and they are often referred to as the Sakhalin-Hokkaido orogenic belt that formed in the early Paleogene (Kodama et al., 2000; Ueda, 2005; 2016; Zharov, 2005; Shigeta and Meada, 2005). Accretionary complexes in both the Sakhalin and Hokkaido Islands are intruded by the Eocene granitoids (Table 1; Kemp et al., 2007; Jahn et al., 2014; Liao et al., 2018). In the offshore to the east of the Sakhalin Island, an ophiolitic mélange was identified, which was considered as a suture zone between the Okhotsk Sea Plate and the Eurasia Plate (Worrall et al., 1996; Piip and Rodnikov, 2004; Rodnikov et al., 2013). Therefore, building of the Sakhalin-Hokkaido orogenic belt might also evolve docking of the Okhotsk Sea Plate to the Eurasia Plate.

Eocene is the most important period for the Sakhalin-Hokkaido orogenic belt as several tectonic events occurred in the Eocene may affect its formation and related magmatism. The first event is the cessation of subduction along the Sakhalin and Hokkaido Islands. The cessation of subduction was caused by collision of island arcs (Osanai et al., 1991; Zharov, 2005) or the Okhotsk Sea Plate (Jolivet et al., 1988; Maruyama et al., 1997; Taira, 2001; Zhao et al., 2018) to the eastern margin of the Eurasia Plate in the Paleocene-Eocene. The second event is the late Paleocene to early Eocene subduction of the Kula-Pacific ridge beneath the Hokkaido Island, which might be responsible for the early Paleogene mafic and granitic intrusion in the Hokkaido Island

(Kimura and Tamaki, 1986; Maeda and Kagami, 1996). The third event is the initial opening of the Japan Sea basin. Based on structural geological and magmatic studies, the initial opening of the Japan Sea basin was assigned to the early Eocene (~50 Ma; Lallemand and Jolivet, 1985/86; Barnes, 2008; Martynov et al., 2017).

How these tectonic events affect formation of the Sakhalin-Hokkaido orogenic belt, especially their contribution to the Eocene magmatism within this belt has not been well studied. In this study, we carried out zircon U-Pb dating, whole-rock elemental and Sr-Nd isotopic studies on granitic rocks from two plutons in the central Sakhalin Island that intruded the East Sakhalin accretionary complex (Fig. 1). The data will be used to constrain the geological setting during their emplacement, and further discuss effects of aforementioned tectonic events on the Sakhalin-Hokkaido orogenic belt.

2. Geological background

The Sakhalin Island is mainly constituted by the West Sakhalin fore-arc basin and the East Sakhalin accretionary complex, separated by the Central Sakhalin Fault (Figs. 1 and 2). The Central Sakhalin Fault is a north-south-trending system of active dextral strike-slip faults with thrust component that transects the Sakhalin Island (Fournier et al., 1994; Seno et al., 1996; Ivashchenko et al., 1997; Weaver et al., 2004), which is also considered as modern plate boundary between the Eurasia Plate and the Okhotsk Sea Plate (e.g., Seno et al., 1996; Takahashi et al., 1999). However, this fault is not the real suture zone between the Eurasia Plate and Okhotsk Sea Plate. The suture zone is located in the eastern offshore of the Sakhalin Island (Worrall et al., 1996). By combination of ophiolitic mélange with blueschist facies metamorphic rocks and gravitational and magnetic anomalies between the northern Sakhalin Basin and the Deryugin Basin in the

Okhotsk Sea, a paleo-subduction zone has been proposed as a result of subduction of the Okhotsk Sea Plate beneath the Sakhalin Island (Rodnikov et al., 2013) and an early Paleogene cessation of this subduction has been suggested (e.g., Kimura, 1994). In this case, the whole Sakhalin Island belongs to the easternmost pre-Eocene margin of the Eurasia Plate and the cessation of subduction was caused by collision of the Okhotsk Sea Plate to the Eurasia Plate (Maruyama et al., 1997).

The West Sakhalin basin is used to be a fore-arc basin associated with the late Cretaceous-Paleogene eastern Sikhote-Alin volcanic belt (Parfenov and Natal'in, 1986; Abrajevitch et al., 2012). It continues to the south and correlates with the Sorachi-Yezo Belt in the Hokkaido Island (Fig. 1; Ueda, 2005; Zharov, 2005; Abrajevitch et al., 2012). Within this basin, more than 5 km-thick Albian to early Paleogene terrigenous sedimentary sequence is well preserved (Fig. 2a; Zharov, 2005; Golozubov et al., 2012; Abrajevitch et al., 2012). The depositional age of this sedimentary sequence has been well defined by marine fossils and magnetostratigraphic studies (Kodama et al., 2000; Golozubov et al., 2012). The Albian-Paleocene terrigenous rocks are overlain by the Eocene-Pliocene clastic sediments, either with a stratigraphic or an angular unconformity (Zharov, 2005; Golozubov et al., 2012).

The East Sakhalin accretionary complex is mainly exposed in the East Sakhalin Mountains and the Tonino-Aniva Peninsula (Fig. 2a). It is composed of Aptian to early Paleogene strongly deformed flysch and turbidite, containing chaotic blocks of chert, limestone, basalt and other rocks of oceanic origin (Zharov, 2005; Zyabrev, 2011; 2015). In some blocks, rocks underwent metamorphism of various degrees up to blueschist facies (Zharov, 2005; Zyabrev, 2011; 2015). Recent detrital zircon U-Pb dating results

from metasedimentary rocks constrained the maximum depositional ages of the accretionary wedge in the late Cretaceous (Campanian) and early Eocene, supporting previous age assignment on the basis of marine fossils (Zhao et al., 2018). Although the East Sakhalin Mountains and the Tonino-Aniva Peninsula have similar rock assemblage, the differences in structure and tectonic positions of individual rock complexes, as well as different Paleogene evolution complicate direct correlation between these two parts (Zharov, 2005). In the East Sakhalin Mountains, the accretionary complex was considered as an accretionary wedge developed along eastern margin of the Eurasian Plate in response to northwestward subduction of the Okhotsk Sea Plate/Paleo-Pacific Plate (e.g., Zyabrev, 2011; 2015; Rodnikov et al., 2013). On the other hand, the accretionary complex in the northern Tonino-Aniva Peninsula (Ozersk terrane) is considered by Zharov (2005) as an exotic oceanic island-arc. Meanwhile, the accretionary complex to the eastern Gulf of Patience in East Sakhalin Island (Fig. 2a), named as the Terpeniya terrane, is also considered as an exotic oceanic island-arc terrane (Glorie et al., 2017). The Ozersk and Terpeniya terranes, together with the Tokoro arc terrane in the Hokkaido Island, were originally an island-arc system formed in the central Pacific Ocean during the late Cretaceous (Zharov, 2005). These arc terranes collided with the Eurasia continental margin during the early Paleocene (Zharov, 2005). However, based on paleomagnetic study in the Ozersk terrane, Bazhenov et al. (2001) proposed that docking of the Ozersk terrane to the Eurasia continental margin occurred around Eocene-Oligocene.

The East Sakhalin accretionary complex was intruded by dispersed granitic plutons. Four early Paleogene peraluminous granitic plutons have been identified by previous

geological mapping, namely the Langeri and Val'za plutons in the central Sakhalin Island, and the Okhotsk and Aniva plutons in the Tonino-Aniva Peninsula (Figs. 1 and 2a). By reviewing previous studies, Khanchuk (2001) considered that these peraluminous granites were collision-related. Zharov (2005) made a detailed investigation on the Aniva pluton and its country rocks (Fig. 1B). The Aniva pluton is made of S-type granite that intruded into strongly deformed accretionary complex during middle Eocene (40.8-34.7 Ma, K-Ar method). Its country rocks show typical collision-related structural features with thermal metamorphic hornfels in the contact zone (Zharov, 2005). Combining the S-type granitic nature of the Aniva pluton, hornfels in the contact zone, and collision-related structure of country rocks, Zharov (2005) considered that the Aniva pluton granites are syncollisional origin. Recently, Liao et al. (2018) reported zircon U-Pb ages of 41-40 Ma for the Aniva pluton, indicating the middle Eocene emplacement of these syncollisional granites.

Both the West Sakhalin fore-arc basin and the East Sakhalin accretionary complex were unconformably overlain by Eocene and younger nonmarine to shallow marine undeformed conglomerates and sandstone (Gladenkov et al., 2000; Zharov, 2005). For the Okhotsk Sea Plate to the east, Eocene sedimentary rocks also overlie basement rocks of the Okhotsk Sea Plate unconformably (Worrall et al., 1996; Lindquist, 2000).

3. Sampling and petrographic description

The Langeri and Val'za plutons in the central Sakhalin Island (Figs. 1 and 2a) were selected for zircon U-Pb dating, whole-rock elemental and isotopic studies. Both two plutons intruded into the late Cretaceous to early Paleogene Verhnelangeri metamorphic complex, which belongs to the western part of the East Sakhalin accretionary complex

(Galversen et al., 2009; Zhao et al., 2018; Fig. 2b). The Verhnelangeri metamorphic complex can be divided into three subcomplexes according to different mineral assemblages and metamorphic grades (Fig. 2b). Detrital zircon dating constrained the maximum depositional ages of black schist and mica-quartz subcomplexes at 49 Ma and 67 Ma, respectively (Zhao et al., 2018). Both plutons are constituted by mainly monzogranite and granodiorite, and no clear boundary between these two rock-types can be found due to heavy burying of the forest. Seven samples were collected from the Langeri pluton and nine samples from the Val'za pluton (Table 2). Figure 3 presents the representative photomicrographs that show mineral phases and textures of studied monzogranite, granodiorite and tonalite. Monzogranite samples show phanerocrystalline texture and consist mainly of quartz, plagioclase, alkali-feldspar and biotite (Fig. 3). Granodiorite samples show phanerocrystalline texture with plagioclase, quartz and biotite as the main minerals and a few alkali-feldspar and hornblende microcrystals (Fig. 3c). Hornblende and biotite of tonalite are usually preserved as euhedral phenocrysts surrounded by microcrystal palgioclase and quartz (Fig. 3d). Both monzogranite and granodiorite sometimes bear minor amount of muscovite (Galversen et al., 2009; Fig. 3). All samples were performed on whole-rock elemental and Sr-Nd isotopic analyses. Two samples from the Langeri pluton and four samples from the Val'za pluton were selected for zircon U-Pb dating. The sampling localities are marked in Fig. 2 and the detailed information for each sample is summarized in Table 2.

4. Analytical Methods

4.1 Zircon U-Pb dating

Zircon grains were separated firstly by conventional heavy liquid combining with magnetic separation technique, followed by handpicking under a binocular microscope at the Regional Geological Survey of Langfang, Hebei Province, China. Handpicked zircons were mounted in epoxy resin bed and half-sectioned and polished when the resin bed had dried. Then, the mounted zircons were photographed under transmitted and reflected light under optical microscope, followed by cathodoluminescence (CL) imaging using a Field Emission Gun Scanning Electron Microscope at Institute of Earth Science (IES), Academia Sinica, Taipei. The CL images will be used for choosing potential target sites for U-Pb analysis. Zircon U-Pb dating was performed using an Agilent 7500s quadrupole ICPMS and a New Wave UP213 laser ablation system at Department of geosciences, National Taiwan University (Chiu et al., 2009). Detailed analytical procedures and operating conditions can be found in Chiu et al. (2009). Element concentrations and isotopic ratios of analyzed zircons were calculated by GLITTER (ver. 4.4.2, Macquarie University; Griffin et al., 2008). Concordia ages and diagrams were acquired using Isoplot/Ex (3.0) (Ludwig, 2003). Common lead was corrected using Andersen's (2002) LA-ICP-MS Common Lead Correction method (ver. 3.15). The data were presented on U-Pb concordia diagrams with errors in 2σ . The weighted mean ages are at 95% confidence levels (Ludwig, 2003).

4.2 Whole-rock elemental analysis

Major element contents were measured using a Rigaku RIX-2000 spectrometer X-ray fluorescence (XRF) spectroscopy on fused glass beads at the Department of Geosciences, National Taiwan Normal University (Lin et al., 2012). For trace element analyses, chemical preparation and mass analysis were carried out at IES, following the

method of Jahn et al. (2014). Firstly, about 200 mg of powdered sample was dissolved in a mixture of HF and HNO₃ (2:1) in a screw-top Savillex Teflon beaker for 5–7 days at 100°C. After this, evaporate the beaker to dryness, then reflux in 6N HCl and dry twice, and finally redissolution the residuum in 1N HCl. Repeating this procedure until complete dissolution was achieved. The final solution was separated into two parts: a small portion (about 12.5 %) was used for further trace element analysis by ICP-MS, and the rest for subsequent chemical separation of Sr and Nd for isotopic analysis. Trace element analysis was performed at the Department of geosciences, National Taiwan University using an Agilent 7500s. Five standard reference materials (AGV-2, BCR-2, BHVO-2, BIR9-1 and DNC-1) were used for trace element analyses. Detailed analytical procedures can be found in Lin et al. (2012). Analytical errors, depending on the concentrations, are 0.5–3% for major elements and 1–10% for trace elements.

4.3 Whole-rock Sr-Nd isotopic analysis

Solutions split after trace element analyses were used for chemical separation of Sr and Nd for isotopic analysis. Detailed procedures for chemical separation and mass analysis can be found in Jahn et al. (2014). Sr and rare-earth elements (REEs) were separated using polyethylene columns packed with a 2.5 ml resin bed of AG 50W-X8 of 100–200 mesh. Nd was separated from other REEs with 1 ml polyethylene columns packed with Eichrom Ln resin (Ln-B25-A) as a cation exchange medium. Sr and Nd isotopes were analyzed using a Finnigan MAT 262 and a TRITON mass spectrometer, respectively at IES. For isotopic analysis, Sr, as well as Nd, was firstly dissolved in a drop of H₃PO₄ and then loaded on a single Re filament (in double-Re-filament configuration). The mass fractionation effect in Sr and Nd isotopic analysis was corrected

by normalizing to $^{86}\text{Sr}/^{88}\text{Sr} = 0.1194$ and $^{146}\text{Nd}/^{144}\text{Nd} = 0.7219$, respectively (Jahn et al., 2014). Analyses of standard NBS-987 Sr and JMC Nd throughout the period of data acquisition yielded $^{86}\text{Sr}/^{87}\text{Sr} = 0.710251 \pm 0.000020$ (2σ external precision) and $^{143}\text{Nd}/^{144}\text{Nd} = 0.511818 \pm 0.000010$ (2σ external precision) (Jahn et al., 2014). Total procedural blanks were ca. 330 pg Sr and 300 pg Nd (Jahn et al., 2014). The internal precision, expressed as $2\sigma_{\text{m}}$, was better than 0.000010 for both Sr and Nd.

5. Analytical results

Results of zircon U-Pb dating are presented in Supplementary Tables S1, and whole-rock chemical and Sr-Nd isotopic data are given in Tables 2 and 3, respectively.

5.1 Zircon U-Pb dating

Zircon grains from all granitic samples are euhedral prismatic in shape and show fine-scale oscillatory growth zoning in CL images (Fig. 4). The uranium concentrations show a large range from 129 to 4457 ppm, with the majority lower than 2000 ppm, and the Th/U ratios range from 0.11 to 0.76 (Supplementary Table S1). Both zircon inner texture and Th/U ratios indicate a magmatic origin for these zircon grains. For each sample, 24 zircon grains were analyzed and the data are illustrated in the concordia plots (Fig. 5). In most cases, data points form tight clusters and yield well-defined $^{206}\text{Pb}/^{238}\text{U}$ ages, which are interpreted as the formation time of these magmatic rocks (Figs. 5a, 5b, 5c and 5f). In some cases, inherited zircon grains can be identified, such as in samples SK15-35 and SK15-39 (Figs. 5d and 5e). However, meaning of these inherited zircons can not be precisely determined.

Two samples from the Langeri pluton give consistent mean $^{206}\text{Pb}/^{238}\text{U}$ age at 37 ± 1 Ma (Fig. 5). Samples from the Val'za pluton also give similar mean $^{206}\text{Pb}/^{238}\text{U}$ ages at 38

± 1 Ma to 36 ± 1 Ma (Fig. 5). The age data indicate that both plutons were emplaced in the late Eocene.

5.2 Whole-rock elemental characteristics

Samples from both two plutons show silica contents in the range of 63 to 76%, and belong to granite and granodiorite in the SiO_2 vs. $\text{Na}_2\text{O}+\text{K}_2\text{O}$ diagram (Fig. 6a). In the Q' vs. ANOR classification (Streckeisen and Le Martre, 1979), all samples except SK15-39 are categorized as granite and granodiorite (Fig. 6b). All granodiorite samples show low $\text{K}_2\text{O}/\text{Na}_2\text{O}$ ratios of 0.47-0.87, whereas granite samples give $\text{K}_2\text{O}/\text{Na}_2\text{O}$ ratios of 0.70-1.11 (Table 3). All monzogranite samples are peraluminous S-type granite in the A/CNK vs. A/NK diagram, whereas granodiorites are both peraluminous I-type to S-type (Fig. 6c; Maniar and Piccoli, 1989). The A/CNK values indicate that although S-type granites are dominant, both S- and I-type granites coexist within each pluton (Fig. 6c). In the $\text{Na}_2\text{O}+\text{K}_2\text{O}-\text{CaO}$ vs. SiO_2 diagram of Frost et al. (2001), they fall in the calc-alkalic and calc fields (Fig. 6d).

Samples from two plutons display very similar chondrite-normalized REE patterns and primitive mantle normalized spidergrams (Fig. 7). They are characterized by enrichment of light REE and near-flat heavy REE, with negative Eu anomalies [$(\text{Eu/Eu}^*)_{\text{N}} = 0.12-0.82$] (Fig. 7). The $(\text{La/Yb})_{\text{N}}$ ratios vary from 4.4 to 9.1. In the spidergrams, they show enrichment of Cs, Rb, Th and U, and depletion in Ba, Nb, Ta, P and Ti (Fig. 7). The enrichment-depletion patterns of these elements are similar with those of arc-related granitoids in the Sikhote-Alin orogenic belt (Jahn et al., 2015) and S-type granites in the southern Sakhalin Island (Liao et al., 2018), whereas differentiation degrees of these elements are relatively insignificant comparing with those of typical S-

type granite in the Himalayas (e.g., Guo and Wilson, 2012). In the classification diagram of Whalen et al. (1987), they belong to the unfractionated granite (Fig. 8).

5.3 Whole-rock Sr-Nd isotopic data

Whole-rock Sr and Nd isotopic data are given in Table 4 and presented in Fig. 9. The Rb and Sr concentrations range from 34 to 172 ppm and from 50 to 411 ppm, respectively (Table 4). The calculated initial $^{87}\text{Sr}/^{86}\text{Sr}$ ratios (I_{Sr} values) show consistent values from 0.7042 to 0.7049 and the $\varepsilon_{\text{Nd}}(t)$ values vary from +1.7 to +3.1 (Table 4 and Fig. 9). Granitic samples have single-stage Sm-Nd model ages of 673 to 817 Ma and two-stage model ages of 611 to 717 Ma (Table 4).

6. Discussion

6.1 Eocene magmatism in the Sakhalin and Hokkaido Islands

The new zircon U-Pb ages obtained in this study revealed the late Eocene (38-36 Ma) emplacement for the two granitic plutons. These ages are similar with those obtained from the Aniva pluton in the southern Tonino-Aniva Peninsula, where two K-Ar ages have been reported at 40.8 and 34.7 Ma, respectively (Zharov, 2005). Recently, Liao et al. (2018) and Alexandrov et al. (2018) performed zircon U-Pb dating on the Aniva and Okhotsk plutons in the Tonino-Aniva Peninsula, and the data revealed their emplacement at 41-40 Ma and 44-42 Ma, respectively (Table 1; Fig. 1b). The Eocene granitic rocks were also identified from the Hokkaido Island, which has been considered as the southern extension of the Sakhalin Island (Fig. 1b). Kemp et al. (2007) firstly reported 37.5 Ma granite and tonalite from the Hidaka belt in central Hokkaido Island. Jahn et al. (2014) reported two episodes of granitic intrusions in 46-44 Ma and 37 Ma, respectively, from the Hidaka belt (Table 1; Fig. 1b). These reported isotopic ages indicate that the Eocene

granitoids represent an intense magmatic event along the Sakhalin-Hokkaido orogenic belt.

6.2 Magma sources and petrogenesis

Before using geochemical data to discuss magma sources and petrogenesis, it is worth to note that three granodiorite and one tonalite samples have high LOI values (2.15-3.02 %) and all other samples show low LOI values less than 1.6% (Table 3). For samples with LOI >1% (all of them are granodiorite), we apply CIW diagrams [CIW = $(\text{Al}_2\text{O}_3 / (\text{Al}_2\text{O}_3 + \text{CaO} + \text{Na}_2\text{O})) * 100$, molecular ratio; Harnois, 1988] to determine alteration effects on major element compositions, and use bivariate plots of Zr against other trace elements to evaluate the motilities of trace elements during alteration (e.g., Polat et al., 2002; Zhao et al., 2016). For major elements, SiO₂, Al₂O₃, Fe₂O₃, Na₂O, K₂O, MgO, and TiO₂ show no correlation with CIW, implying insignificant influence of alteration to these major elements (Supplementary Fig. 1). However, CaO shows slightly negative correlation with CIW, indicating the alteration might result in CaO depletion. And K₂O shows slightly positive correlation with CIW, implying that the alteration caused some enrichment of K₂O (Supplementary Fig. 1). The bivariate plots show that REEs (e.g., Lu, Nd and Yb), HFSEs (e.g., Nb and Ta), and most LILEs (e.g., Rb and Ba) are correlated with Zr (Supplementary Fig. 2), indicating essential immobility of these trace elements during alteration. Note that correlation of Sr and Zr are not very good as two samples (SK15-32 and SK15-39) show high Sr content with low Zr contents (Supplementary Fig. 2), implying some degrees of mobility of Sr for these two samples.

Geochemical data reveal that the Langeri and Val'za plutons are dominated by S-type granitoids, with subordinate I-type granitoids based on their high A/CNK values

(Fig. 6c). This kind of combination of Eocene S-type and I-type granites is consistent with coeval granites in the southern Sakhalin Island (Zharov, 2005; Liao et al., 2018) and the Hidaka belt of central Hokkaido Island (Owada and Osanai, 1989; Osanai et al., 1991), but is different from the Cretaceous-Paleocene granitic rocks in the Sikhote-Alin belt, where I-type granites are predominant (Fig. 6c). All samples from two plutons show high normative corundum content, ranging from 1.01 to 3.81 %, which is also a diagnostic characteristic for S-type granite (Table 3; Chappell and White, 2001). Meanwhile, muscovite is the main aluminous-rich mineral for S-type granite of the two plutons (Galversen et al., 2009).

S-type granite is traditionally considered as strongly peraluminous magmas derived dominantly from metasedimentary rocks (metapelites or metagreywacks) (Chappell and White, 1974; Patiño Douce and Harris, 1998; Sylvester, 1998; Collins and Richards, 2008). However, several other models have also been proposed to interpret the petrogenesis of S-type granite including (i) partial melting of biotite-bearing tonalite and granodiorite at pressures $\geq 8\text{ kbar}$ with clinopyroxene in the restite (Patiño Douce, 1997; 1999); (ii) partial melting of basaltic rocks and/or amphibolites under H_2O -saturated conditions (Ellis and Thompson, 1986). Miller (1985) pointed out that very few peraluminous rocks are derived entirely from pelitic sources, instead, a majority is derived from intermediate to felsic crustal sources, including both immature sedimentary rocks and meta-igneous rocks or even metaluminous mafic sources. In recent years, hybrid origin of mantle-derived components with supracrustal components (metasediments) has been proposed for the generation of S-type granites (e.g., Clemens, 2003; Healy et al., 2004; Cai et al., 2011).

The high A/CNK values (1.08-1.14) and high normative corundum contents (1.01-3.81%) for the late Eocene granites strongly support meta-sediments dominated source magma. In the Rb/Sr vs. Rb/Ba diagram, most samples fall between the clay-poor greywacke- and shale-derived sources (Fig. 10a). And in the diagram of $\text{Al}_2\text{O}_3/(\text{MgO}+\text{FeO}^T)$ vs. $\text{CaO}/(\text{MgO}+\text{FeO}^T)$, all samples were plotted in the areas of partial melts from metagraywackes and metabasaltic to metatonitic sources (Fig. 10b). Patiño Douce (1999) summarized experimental granitic liquids produced by melting of felsic pelites (muscovite schists), metagreywackes and amphibolites. Our monzogranite samples fall mainly in the range of the metagreywackes-derived melts and granodiorite samples fall in the field of amphibolites-derived melts (Figs. 10c and 10d), indicating that granites from both two plutons were derived from remelting of metasediments and amphibolites in the accretionary complex. The low $\text{K}_2\text{O}/\text{Na}_2\text{O}$ ratios of granodiorite (0.47-0.87) and some granite (0.70-1.11) also argue for the role of metabasitic substrates in the source of granitoids. This consideration is consistent with that of the late Eocene peraluminous granites from the Hidaka belt in central Hokkaido Island. From mineralogical and chemical characteristics, combined with metamorphic conditions, the late Eocene peraluminous S-type granites in the Hidaka belt were considered to have been derived from crustal anatexis of pelitic to psammitic metamorphic rocks in the lower crust (Owada, 1989; Osanai et al., 1991; Shimura et al., 1992). In contrast, the coeval I-type granites were thought to have been derived from crustal anatexis of pyroxene amphibolites in the lower crust (Shimura et al., 1992). Meanwhile, S- and I-type granites from both the Sakhalin and Hokkaido Islands show typical arc magma signatures, including enrichment of light-REE, negative Eu, and Ta-Nb-Ti anomalies.

(Fig. 8; Jahn et al., 2014; Liao et al., 2018). The arc-like affinity can be well explained by the anatexis of subduction-related accretionary complexes.

All samples in this study show consistent Sr-Nd isotopic data, with unified initial Sr ratios of 0.7042 to 0.7049, and positive $\varepsilon_{\text{Nd}}(t)$ values from +1.7 to +3.1 (Fig. 9). The $\varepsilon_{\text{Nd}}(t)$ values are much lower than that of the depleted mantle, implying old crustal contribution in the granite petrogenesis. Detrital zircon U-Pb dating reveals abundant Precambrian and Paleozoic recycled zircon grains from Miocene sandstone in the West Sakhalin basin and meta-sedimentary rocks in the East Sakhalin accretionary complex, which was interpreted to be originated from northeastern Asia continent (Zhao et al., 2017b; 2018). Input of these old materials might be responsible for the low $\varepsilon_{\text{Nd}}(t)$ values of the late Eocene granites. Isotopic studies on the late Eocene S- and I-type granites in the Hidaka belt showed initial Sr isotopic ratios in the range of 0.7048 to 0.7065, and 0.7033 to 0.7048, respectively, and these ratios are nearly identical to the ranges of pelitic metamorphic rocks (0.7043 to 0.7063) and of pyroxene amphibolites (0.7029 to 0.7049), respectively (Owada and Osanai, 1989; Ikeda, 1991; Shimura et al., 1992). The isotopic data also support anatexis of pelitic metamorphic rocks and amphiolites in the generation of S- and I-type granites in the Hidaka belt (Shimura et al., 1992). Sr-Nd isotopic features of the Langeri and Val'za plutons in the central Sakhalin Island (this study) and the Okhotsk and Aniva plutons in southern Sakhalin Island (Liao et al., 2018) show consistent values with those from the Hokkaido Island (Fig. 9), indicating similar source nature for these late Eocene granitic rocks. The East Sakhalin accretionary complex can be well correlated with the Hidaka belt in central Hokkaido Island in both ages and compositions (Fig. 1; Zharov, 2005). Therefore, we may assume that the East Sakhalin

accretionary belt and the Hidaka belt share the same Sr-Nd isotopic characteristics, and tentatively propose that granites of both Langeri and Val'za plutons were derived from anatexis of metasediments and amphibolites of the East Sakhalin accretionary complex.

In the Hidaka belt, large volumes of early Paleogene gabbro plutons have been identified accompanying with coeval granitic plutons (Meada, 1990). Meada and Kagami (1994) considered that intrusion of these mafic plutons provided heat sources for anatexis of accretionary complex, which led to the formation of coeval granitic plutons. By further elemental and Sr-Nd isotopic studies of these gabbros, Maeda and Kagami (1996) found that mafic plutons show MORB-like geochemical characteristics and a derivation from primitive basaltic magma for these mafic rocks has been proposed. Considering the nearly synchronous arrival of the Kula-Pacific ridge, Maeda and Kagami (1996) suggested that upwelling of asthenospheric mantle in a spreading ridge setting is responsible for the formation of MORB-like gabbros and anatexis of the accretionary prism. For the East Sakhalin accretionary complex, no Eocene mafic intrusion has been reported. However, diorite enclaves have been identified from Eocene granitic plutons (Liao et al., 2018). These enclaves display initial Sr isotopic ratios of 0.7044 and 0.7050 and $\varepsilon_{\text{Nd}}(t)$ values of +1.9 and +3.4 (Liao et al., 2018), consistent with those from hosting granites. These values fall in-between those of MORB-like gabbros and accretionary complex from the Hidaka belt (Maeda and Kagami, 1996). Therefore, we may assume that there might also be mafic intrusions beneath the Sakhalin Island and these mafic intrusions not only provide heat source for anatexis of accretionary complex, but also supply juvenile materials during formation of granitic plutons in the Sakhalin Island.

Note that strong fractional crystallization of calc-alkaline liquid in which plagioclase and hornblende (and biotite) were separated can elevate the A/CNK value from metaluminous to slightly peraluminous ($1 < \text{A/CNK} < 1.1$) (Jahn et al., 2001) and these rocks are usually classified as fractionated I-type granite. But this process can hardly produce S-type granite with $\text{A/CNK} > 1.1$. All I-type granitic samples in this study belong to unfractionated granite in the FeO/MgO vs. $\text{Zr}+\text{Nb}+\text{Ce}+\text{Y}$ diagram (Fig. 8). Meanwhile, A/CNK values display no positive correlation with SiO_2 contents, also indicating low degree of fractional crystallization. Therefore, strong fractional crystallization of calc-alkaline liquid can be excluded for the peraluminous nature of I-type granite in this study. Nevertheless, some degrees of fractional crystallization should have occurred during magma differentiation as in both Ba vs. Sr and Rb/Sr vs. Sr diagrams (Figs. 10e and 10f), fractionation of plagioclase and K-feldspar can be observed, which can also explain the depletion of Ba-Sr-Eu in the spidergrams (Fig. 7).

6.3 Possible mechanisms for generation of the Eocene granites

A key factor in formation of S-type granite is to have a metasedimentary or metabasaltic source buried in the deep crust before anatexis, and many researchers prefer continental collision that can easily cause crust thickening to achieve this (Barbarin, 1998; Collins and Richards, 2008). One good example of continental collision deduced S-type granites is the leucogranites in the Himalaya Mountain produced by India-Asia collision (e.g., Le Fort et al., 1987; Inger and Harris, 1993). However, only a few of S-type granites occurring in all the Phanerozoic circum-Pacific orogens have undergone any form of continental collision (Collins and Richards, 2008). On the contrary, in the circum-Pacific orogens, most S-type granites were emplaced under specific geodynamic

conditions associated with arc-arc collision (Osanai et al., 1991), back-arc extension (e.g., Collins and Richards, 2008), continental margin strike-slip (Kruk et al., 2014), or extension after a period of contraction during accretion (Healy et al., 2004).

The Hokkaido Island was built by collision of two Cretaceous arc-trench systems along the Hidaka metamorphic belt in the early Paleogene (Komatsu et al., 1989; Osanai et al., 1991; Ueda, 2016). This collisional event caused tectonic thickening of accreted terrigenous and oceanic crustal rocks, which was responsible for the formation of late Eocene peraluminous granites in the Hidaka belt (Osanai et al., 1991). Contemporaneous collision also occurred in the southern Sakhalin Island. The Ozersk terrane, an island arc, accreted to the Eurasia continental margin (represented by the West Sakhalin fore-arc basin) in the early Paleogene (Zharov, 2005). The accretion-related imbricate structure in the suture zone is overlain unconformably by the late Eocene-Oligocene sediments, postdating this accretionary event (Zharov, 2005). This accretion caused thickening of accretionary complex (Zharov, 2005), and partial melting of accreted metasediments and oceanic crustal materials might be responsible for the formation of S- and I-type granites in the southern Sakhalin Island (Liao et al., 2018).

In the early Paleogene, an independent plate, named Okhotsk Sea Plate or Okhotomorsk Block, arrived at the eastern margin of NE Asia and welded with the Eurasia Continent along the suture zone beneath the eastern offshore of Sakhalin Island (Maruyama et al., 1997; Rodnikov et al., 2013). This continental welding caused the subduction front jumping eastward to the Kuril Arc (Jolivet, 1987; Kimura, 1994; Rodnikov et al., 2013; Piip and Rodnikov, 2004). Recent zircon dating result constrained that welding of the two plates occurred in the middle Eocene (Zhao et al., 2018).

Continental welding caused strong deformation of the West Sakhalin fore-arc basin, the East Sakhalin accretionary complex, as well as their geological equivalents in the Hokkaido Island. In the Hokkaido Island, present-day structural polarity is westward convergence, and Taira (2001) interpreted this structural polarity owing to the collision of the Okhotsk Sea Plate to the Eurasia continent during the Paleogene. In the Sakhalin Island, many top-to-west thrust faults have been identified (Galversen et al., 2009), these thrusts and related folds can also be ascribed to the collision of the Okhotsk Sea Plate to the Eurasia continent. The continental welding also caused thickening of continental crust beneath the Sakhalin and Hokkaido Islands (Golozubov, 2006; Rodnikov et al., 2014), triggering anatexis of metasediments and amphibolites in lower crust, which leads to the emplacement of the late Eocene granitic plutons intruded the East Sakhalin accretionary complex. Therefore, we can conclude that the late Eocene granites in the Sakhalin Island were generated in a syn-collisional tectonic setting related to the collision of the Okhotsk Sea Plate to the Eurasia continent. Although we think the continental welding model is the most plausible mechanism for generation of the Eocene magmatism, two other Eocene tectonic events may also contribute to the Eocene magmatism. As aforementioned, late Paleocene to Early Eocene subduction of the Kula-Pacific ridge beneath the Hokkaido Island was considered to be responsible for the early Paleogene mafic and granitic intrusion in the Hokkaido Island (Kimura and Tamaki, 1986; Maeda and Kagami, 1996). However, direction of this ridge subduction is nearly perpendicular with the Sakhalin-Hokkaido orogenic belt (Mawda and Kagami, 1996). This kind of ridge subduction can supply large volume of mafic magma beneath the Hokkaido Island and provide heat source to melt accretionary prism. But the Sakhalin Island is not close to the

subducting ridge, and mafic magma may not reach the Sakhalin Island, so the heat transferred to the Sakhalin Island is not as much as that to the Hokkaido Island. This may explain the fact that Eocene mafic intrusions are rare in the Sakhalin Island and volume of granitoids in the Sakhalin Island is much less than that in the Hokkaido Island.

From structure geological investigation of the Hokkaido Central Belt and marine geology studies along the eastern margin of the Japan Sea, the early Eocene-Oligocene rifting of small pull-apart basins accommodating two large dextral shear zone (east of Korea and west of Hokkaido-Sakhalin) has been proposed. The initial rifting caused eruption of the early Eocene high alkali volcanic rocks in South Korea and Southwest Japan, and late Eocene granitic intrusions and volcanic extrusions in the Tohoku-Hokkaido may also related to this event (Barnes, 2008). The initial rifting of the pull-apart basins is controlled by strike-slip fault system. Lallemand and Jolivet (1985/86) considered that dextral movement along the Yangsan-Tsushima fault system and the Tertiary-Hidaka shear zone begins in the middle Eocene, producing small pull-apart basins along shear zone in northern Kyushu and Hokkaido. These pull-apart basins may favor the ascending of magma. Similarly, based on paleomagnetic studies, Weaver et al. (2003) proposed a transpressive regime for the Sakhalin Island around the middle-late Eocene due to the dextral strike-slip movement of the Central Sakhalin Fault. However, whether the emplacement of the late Eocene granitic plutons is related to this dextral strike-slip movement is still unclear. Meanwhile, structural geological studies argued that the activity of the Central Sakhalin Fault started from the Miocene rather than the middle-late Eocene (Jolivet, 1987; Fournier et al., 1994). In this case, the strike-slip transpression has no relationship with emplacement of the late Eocene granites. Therefore, more

studies are needed to uncover the relationship of strike-slip movement and emplacement of Eocene magmatic rocks in the Sakhalin-Hokkaido orogenic belt.

7. Conclusions

Based on the newly obtained geochronological, elemental and Sr-Nd isotopic data, we reach the following conclusions:

- (1) Zircon U-Pb dating revealed that the Langeri and Val'za plutons in the central Sakhalin Island emplaced in the late Eocene (38-36 Ma).
- (2) Whole-rock elemental data indicate that granitoids are mainly peraluminous S-type with subordinate I-type granite, and they show arc-like geochemical affinities. Sr-Nd isotopic results show consistent low initial $^{87}\text{Sr}/^{86}\text{Sr}$ ratios, positive $\varepsilon_{\text{Nd}}(t)$ values and young Nd model ages. Elemental and isotopic data reveal that S- and I-type granitic rocks of the Langeri and Val'za plutons are generated from remelting of metasediments and amphibolites in the accretionary complex.
- (3) The late Eocene granitic rocks were generated in a syn-collisional tectonic setting. The middle-late Eocene welding of the Okhotsk Sea Plate and the Eurasia Continent is the most plausible mechanism that caused crustal thickening beneath the Sakhalin Island, and anatexis of metasediments and oceanic crustal materials in lower crust is responsible for the formation of late Eocene granitic rocks.
- (4) Late Paleocene to early Eocene subduction of the Kula-Pacific ridge beneath the Hokkaido Island and Eocene initial rifting of pull-apart basins along strike-slip fault system may also contribute to the emplacement of Eocene magmatism in the Sakhalin-Hokkaido orogenic belt.

Acknowledgements

We thank Dr. Sergei Lavrik for his support and guidance during the 2015 field excursion in the Sakhalin Island. We appreciate the kind help from Miss. Shu-chen Chiu for zircon CL imaging and U-Pb dating. We are deeply grateful to Ms. Masako Usuki (National Taiwan University) and Mr. Wen-Yu Hsu (IES, Academia Sinica) for their help in Sr-Nd chemical separation and isotope analyses. Pan Zhao is indebted to the Ministry of Science and Technology (MOST) of Taiwan for post-doctoral fellowship. Bor-ming Jahn acknowledges the support of the MOST through grants MOST 104-2116-M-002-004, MOST 105-2116-M-002-007 and MOST 105-2923-M-002-002. Research Projects of Russian Found of Basic Research (No. 15-55-52035) and Far East Branch of Russian Academy of Sciences (No. 15-I-2-004) are acknowledged by Igor Alexandrov and Vitaly Ivin. We gratefully acknowledge the Editor Prof. Nelson Eby for handling this paper and two anonymous reviewers for reviewing and providing constructive comments that helped us to improve the manuscript.

Reference

- Abrajevitch, A., Zyabrev, S., Didenko, A.N., Kodama, K., 2012. Palaeomagnetism of the West Sakhalin Basin: evidence for northward displacement during the Cretaceous. *Geophysical Journal International* 190, 1439–1454.
- Akinin, V.V., and Miller, E.L., 2011. Evolution of Calc-Alkaline Magmas of the Okhotsk–Chukotka Volcanic Belt. *Petrology* 19(3), 237-277.
- Alexandrov, I. A., Liao, J.-P., Jahn, B.-M., Golozubov, V. V., Ivin, V. V., Stepnova, Yu.A., 2018. Eocene age of granitoids of Okhotsk granodiorite complex (Southern Sakhalin). *Doklady Earth Sciences*, in press.
- Altherr, R., Holl, A., Hegner, E., Langer, C., Kreuzer, H., 2000. High-potassium, calc-alkaline I-type plutonism in the European Variscides: northern Vosges (France) and northern Schwarzwald (Germany). *Lithos* 50, 51–73.
- Andersen, T., 2002. Correction of common lead in U-Pb analyses that do not report ^{204}Pb . *Chemical Geology* 192, 59–79.
- Barbarin, B., 1998. A review of the relationships between granitoid types, their origins and their geodynamic environments. *Lithos* 46, 605–626, doi:10.1016/S0024-4937(98)00085-1.
- Barnes, G.L., 2008. The Making of the Japan Sea and the Japanese Mountains: Understanding Japan’s Volcanism in Structural Context. *Japan Review* 20, 3-52.
- Bazhenov, M.L., Zharov, A.E., Levashova, N.M., Kodama, K., Bragin, N.Y., Fedorov, P.I., Bragina, L.G., Lyapunov, S.M., 2001. Paleomagnetism of a Late Cretaceous island arc complex from South Sakhalin, East Asia: Convergent boundaries far away

from the Asian continental margin? *Journal of Geophysical Research* 106, 19193-19205.

Cai, K., Sun, M., Yuan, C., Zhao, G., Xiao, W., Long, X., Wu, F., 2011. Geochronology, petrogenesis and tectonic significance of peraluminous granites from the Chinese Altai, NW China. *Lithos* 127, 261-281.

Chappell, B.W., and White, A.J.R., 1974. Two contrasting granite types. *Pacific Geology* 8, 173-4.

Chiu, H.Y., Chung, S.L., Wu, F.Y., Liu, D., Liang, Y.H., Lin, I.J., Iizuka, Y., Xie, L.W., Wang, Y., Chu, M.F., 2009. Zircon U-Pb and Hf isotopic constraints from eastern Transhimalayan batholiths on the pre-collisional magmatic and tectonic evolution in southern Tibet. *Tectonophysics* 477, 3-19.

Clemens, J.D., 2003. S-type granitic magmas—petrogenetic issues, models and evidence. *Earth-Science Reviews* 61, 1-18.

Collins, W.J., and Richards, S.W., 2008. Geodynamic significance of S-type granites in circum-Pacific orogens. *Geology* 36, 559-562, doi: 10.1130/G24658A.1

DePaolo, D.J., 1988. *Neodymium Isotope Geochemistry An Introduction*. Springer-Verlag, New York, 187 pp.

Ellis, D.J., Thompson, A.B., 1986. Subsolidus and partial melting reactions in the quartz excess CaO+MgO+Al₂O₃+SiO₂+H₂O system under water-excess and waterdeficient condients to 10 kb: some implications for the origin of peraluminous melts from mafic rocks. *Journal of Petrology* 27, 91–121.

- Filatova, N.I., 2015. Transform Margin Maastrichtian–Paleogene Magmatism in East Asia: the Problem of “Belts” in the Koryak–Western Kamchatka Region. *Petrology* 23(4), 331–352.
- Fournier, M., Jolivet, L., Huchon, P., 1994. Neogene strike-slip faulting in Sakhalin and the Japan Sea opening. *Journal of Geophysical Research* 99, 2701–2725.
- Frost, B.R., Barnes, C.G., Collins, W.J., Arculus, R.J., Ellis, D.J., Frost, C.D., 2001. A geochemical classification for granitic rocks. *Journal of Petrology* 42, 2033–2048.
- Galversen, V.G., Evseev, S.V., Konovalenko, A.A., Khaibullina, G.A., 2009. State Geological Map of the Russian Federation, scale 1:200 000, second ed. Sakhalin series. Sheet M-54-XVIII (Pogranichnoye). Explanatory note. St. Petersburg. VSEGEI Publishing. (in Russian).
- Gladenkov, A.Y., White, L.D., Gladenkov, Y.B., Blueford, J.R., 2000. Cenozoic biostratigraphy of the Pogranichnyi Region, Eastern Sakhalin, Russia. *Palaeogeography, Palaeoclimatology, Palaeoecology*, 158(1-2), 45–64.
- Glorie, S., Alexandrov, I.A., Nixon, A., Jepson, G., Gillespie, J., Jahn, B.-M., 2017. Thermal and exhumation history of Sakhalin Island (Russia) constrained by apatite U-Pb and fission track thermochronology. *Journal of Asian Earth Sciences* 143, 326–342.
- Goldstein, S.L., Onions, R.K. Hamilton, P.J., 1984. A Sm-Nd Isotopic Study of Atmospheric Dusts and Particulates from Major River Systems. *Earth and Planetary Science Letters* 70(2), 221–236.
- Golozubov, V.V., 2006. Tectonics of the Jurassic and Lower Cretaceous Complexes of the North-Western Framing of Pacific Ocean. Dal'nauka, Vladivostok, 239 p. (in Russian).

- Golozubov, V.V., Kasatkin, S.A., Grannik, V.M., Nechayuk, A.E., 2012. Deformation of the Upper Cretaceous and Cenozoic Complexes of the West Sakhalin Terrane. *Geotectonics* 46, 333–351.
- Grebennikov, A.V., Khanckuk, A.I., Gonevchuk, V.G., Kovalenko, S.V., 2016. Cretaceous and Paleogene granitoid suites of the Sikhote Alin area (Far East Russia): Geochemistry and tectonic implications. *Lithos* 261, 250-261.
- Griffin, W.L., Powell, W.J., Pearson, N.J., O'Reilly, S.Y., 2008. GLITTER: data reduction software for laser ablation ICP-MS. In: Sylvester, P., (Ed.), *Laser Ablation-ICP-MS in the Earth Sciences*, Mineralogical Association of Canada Short Course Series Volume 40, Appendix 2, pp. 204–207.
- Guo, Z., and Wilson, M., 2012. The Himalayan leucogranites: Constraints on the nature of their crustal source region and geodynamic setting. *Gondwana Research* 22, 360-376.
- Harnois, L., 1988. The CIW index: a new chemical index of weathering. *Sedimentary Geology* 55, 319–322.
- Healy, B., Collins, W.J., Richards, S.W., 2004. A hybrid origin for Lachlan S-type granites: the Murrumbidgee Batholith example. *Lithos* 78, 197-216.
- Ikeda, Y., 1991. Geochemistry and magmatic evolution of Pliocene-early Pleistocene pyroclastic flow deposits in central Hokkaido, Japan. *J. Geol. Soc. Japan* 97, 645- 66.
- Inger, S., and Harris, N., 1993. Geochemical Constraints on Leucogranite Magmatism in the Langtang Valley, Nepal Himalaya. *Journal of Petrology* 34, 345-368, doi: 10.1093/petrology/34.2.345

- Ivashchenko, A.I., Kim, C.U., Oscorbin, L.S., Poplavskaya, L.N., Poplavskiy, A.A., Burymskaya, R.N., Mikhailova, T.G., Vasilenko, N.F., Streltsov, M.I., 1997. The Neftegorsk, Sakhalin Island, earthquake of 27 May 1995. *Isl. Arc* 6, 288-307.
- Jacobsen, S.B., and Wasserburg, G.J., 1980. Sm-Nd isotopic evolution of chondrites. *Earth and Planetary Science Letters* 50, 139-155.
- Jahn, B.M., Wu, F., Capdevila, R., Martineau, F., Zhao, Z., Wang, Y., 2001. Highly evolved juvenile granites with tetrad REE patterns: the Woduhe and Baerzhe granites from the Great Xing'an Mountains in NE China. *Lithos* 59, 171-198.
- Jahn, B.M., Usuki, M., Usuki, T., Chung, S.L., 2014. Generation of Cenozoic granitoids in Hokkaido (Japan): constraints from zircon geochronology, Sr–Nd–Hf isotopic and geochemical analyses, and implications for crustal growth. *American Journal of Science* 314, 704–750.
- Jahn, B.M., Valui, G., Kruk, N., Gonevchuk, V., Usuki, M., Wu, J.T.J., 2015. Emplacement ages, geochemical and Sr–Nd–Hf isotopic characterization of Mesozoic to early Cenozoic granitoids of the Sikhote-Alin Orogenic Belt, Russian Far East: Crustal growth and regional tectonic evolution. *Journal of Asian Earth Sciences* 111, 872-918.
- Jolivet, L., 1987. America-Eurasia plate boundary in eastern Asia and the opening of marginal basins. *Earth and Planetary Science Letters* 81(2-3), 282-288, doi: 10.1016/0012-821X(87)90164-6.
- Jolivet, L., Cadet, J.P., Lalevee, F., 1988. Mesozoic evolution of Northeast Asia and the collision of the Okhotsk microcontinent. *Tectonophysics* 149(1-2), 89-109.

- Kemp, A.I.S., Shimura, T., Hawkesworth, C.J., 2007. Linking granulites, silicic magmatism, and crustal growth in arcs: Ion microprobe (zircon) U-Pb ages from the Hidaka metamorphic belt, Japan. *Geology* 35, 807–810, doi: 10.1130/G23586A.1.
- Khanchuk, A.I., 2001. Pre-Neogene tectonics of the Sea-of-Japan region: a view from the Russian side. *Earth Sci. (Chikyu Kagaku)* 55, 275–291.
- Khanchuk, A.I., Kemkin, I.V., Kruk, N.N., 2016. The Sikhote-Alin orogenic belt, Russian South East: terranes and the formation of continental lithosphere based on geological and isotopic data. *Journal of Asian Earth Sciences* 120, 117–138.
- Kimura, G., 1994. The latest Cretaceous-early Paleogene rapid growth of accretionary complex and exhumation of high pressure series metamorphic rocks in northwestern Pacific margin. *Journal of Geophysical Research* 99, 22147-22164.
- Kimura, G., and Tamaki, K., 1986. Tectonic framework of the Kuril arc since its initiation, in Nasu, N., et al., eds., *Formation of active ocean margins*: Tokyo, Terra, p. 641–676.
- Kodama, K., Meada, H., Shigeta, Y., Kase, T., Takeuchi, T., 2000. Magnetostratigraphy of Upper Cretaceous strata in South Sakhalin, Russian Far East. *Cretaceous Research* 21, 469–478.
- Komatsu, M., Osanai, Y., Toyoshima, T., Miyashita, S., 1989. Evolution of the Hidaka Metamorphic Belt, northern Japan. In: *Evolution of Metamorphic Belts* (eds Daly, J. S., Cliff, R. A. & Yardley, B. W. D.), Geological Society Special Publication 43, 487-493.
- Kruk, N.N., Simanenko, V.P., Gvozdev, V.I., Golozubov, V.V., Kovach, V.P., Serov, P.I., Kholodnov, V.V., Moskalenko, E.Yu., Kuibida, M.L., 2014. Early Cretaceous

- granitoids of the Samarka terrane (Sikhote-Alin): geochemistry and sources of melts. *Russian Geology and Geophysics* 55, 216–236.
- Lallemand, S., and Jolivet, L., 1985/86. Japan Sea: a pull-apart basin?. *Earth and Planetary Science Letters* 76, 375-389.
- Le Fort, P., Cuney, M., Deniel, C., France-Lanord, C., Sheppard, S.M.F., Upreti, B.N., Vidal, P., 1987. Crustal generation of the Himalayan leucogranites. *Tectonophysics* 134, 39-57, doi:10.1016/0040-1951(87)90248-4
- Leonova, V.V., Akinin, V.V., Alshevsky, A.V., Polzunenkov, G.O., 2015. New Localities of Cenozoic Alkali Basalts with Mantle Xenoliths in Northern Okhotsk Region (Seimkan Field). *Russian Journal of Pacific Geology* 9(4), 287–300.
- Liao J.P., Jahn B.-M., Alexandrov I., Chung S.-L., Zhao P., Ivin V., Usuki T. 2018. Petrogenesis of Mid-Eocene granites in South Sakhalin, Russian Far East: juvenile crustal growth and comparison with granitic magmatism in Hokkaido and Sikhote-Alin. *Journal of Asian Earth Sciences*, doi: <https://doi.org/10.1016/j.jseas.2018.05.020>.
- Lin, I.J., Chung, S.L., Chu, C.H., Lee, H.Y., Gallet, S., Wu, G., Ji, J., Zhang, Y., 2012. Geochemical and Sr–Nd isotopic characteristics of Cretaceous to Paleogene granitoids and volcanic rocks, SE Tibet: petrogenesis and tectonic implications. *Journal of Asian Earth Sciences* 53, 131–150.
- Lindquist, S.J., 2000. The North Sakhalin Neogene Total Petroleum System of Eastern Russia. USGS Open-File Report 99-50-O, 1-18.

- Luchitskaya, M.V., and Soloviev, A.V., 2012. Early Eocene Magmatism in the Sredinnyi Range, Kamchatka: Composition and Geodynamic Aspects. *Petrology* 20(2), 147-187.
- Ludwig, K.R., 2003. User's manual for Isoplot 3.0: a geochronological toolkit for Microsoft Excel. Berkeley Geochronology Center, Special Publication, 4pp. 1–71.
- Lugmair, G.W., and Marti, K., 1978. Lunar initial $^{143}\text{Nd}/^{144}\text{Nd}$: differential evolution of the lunar crust and mantle. *Earth and Planetary Science Letters* 39, 349-357.
- Maeda, J., 1990. Opening of the Kuril Basin deduced from the magmatic history of central Hokkaido, North Japan. *Tectonophysics* 174, 235–255.
- Maeda, J., and Kagami, H., 1994. Mafic igneous rocks derived from N-MORB source mantle, Hidaka magmatic zone, central Hokkaido: Sr and Nd isotopic evidence. *Geological Society of Japan Journal* 100, 185–188.
- Maeda, J., and Kagami, H., 1996. Interaction of a spreading ridge and an accretionary prism: Implications from MORB magmatism in the Hidaka magmatic zone, Hokkaido, Japan. *Geology* 24, 31–34.
- Maniar, P.D., Piccoli, P.M., 1989. Tectonic discrimination of granitoids. *Geological Society of American, Bulletin* 101, 635– 643.
- Martynov, Y.A., Khanchuk, A.I., Grebennikov, A.V., Chashchin, A.A., Popov, V.K., 2017. Late Mesozoic and Cenozoic volcanism of the East Sikhote-Alin area (Russian Far East): A new synthesis of geological and petrological data. *Gondwana Research* 47, 358-371.

- Maruyama, S., Isozaki, Y., Kimura, G., Terabayashi, M., 1997, Paleogeographic maps of the Japanese Islands: Plate tectonic synthesis from 750 Ma to the present: The Island Arc 6, 121-142.
- Miller, C.F., 1985. Are strongly peraluminous magmas derived from pelitic sediment sources? Journal of Geology 93, 673-689.
- Osanai, Y., Komatsu, M., Owada, M., 1991. Metamorphism and granite genesis in the Hidaka Metamorphic Belt, Hokkaido, Japan. Journal of metamorphic Geology 9, 111-124.
- Owada, M., 1989. Geology and chemical composition of granitic rocks in the southern part of the Hidaka metamorphic belt, with special reference to cordierite-bearing granitic rocks. Journal of Geological Society of Japan 95, 227-240 (in Japanese with English abstract).
- Owada, M., and Osanai, Y., 1989. Genesis of granite in the Hidaka Metamorphic Belt. Earth Mon 11, 252-7.
- Parfenov, L.M., Natal'in, B.A., 1986. Mesozoic tectonic evolution of northeastern Asia. Tectonophysics 127, 291–304.
- Patiño Douce, A.E., 1997. Generation of peraluminous A-type granites by low-pressure melting of calc-alkaline granitoids. Geology 25, 743–766.
- Patiño Douce, A.E., 1999. What do experiments tell us about the relative contributions of crust and mantle to the origins of granitic magmas? In: Castro, A., Fernandez, C., Vigneresse, J.L. (Eds.), Understanding granites: intergrating new and classical techniques. Geological Society of London, Special Publications 168, 55– 75.

- Patiño Douce, A.E., Harris, N., 1998. Experimental constraints on Himalayan anatexis. *Journal of Petrology* 39, 689–710.
- Piip, V.B., and Rodnikov, A.G., 2004. The Sea of Okhotsk crust from deep seismic sounding data. *Russian Journal of Earth Sciences* 6(1), 35-48.
- Polat, A., Hofmann, A.W., Rosing,M.T., 2002. Boninite-like volcanic rocks in the 3.7–3.8 Ga Isua greenstone belt, West Greenland: geochemical evidence for intraoceanic subduction zone processes in the early Earth. *Chemical Geology* 184, 231–254.
- Rodnikov, A.G., Sergeyeva, N.A., Zabarinskaya, L.P., 2013. Ancient subduction zone in Sakhalin Island. *Tectonophysics* 600, 217–225.
- Rodnikov, A.G., Sergeyeva, N.A., Zabarinskaya, L.P., 2014. Crustal and mantle structure of the Sea of Okhotsk, Pacific Northwest: A review. *Episodes* 37, 312-316.
- Sengör, A.M.C., Natal'in, B.A., 1996. Turkic-type orogeny and its role in the making of the continental crust. *Annual Review of Earth Planetary Sciences* 24, 263–337.
- Seno, T., Sakurai, T., Stein, S., 1996. Can the Okhotsk plate be discriminated from the North American plate? *Journal of Geophysical Research* 101, 11305– 11315.
- Shigeta, Y., and Meada, H., 2005. Yezo Group Research in Sakhalin-A Historical Review. In: Shigeta, Y., and Meada, H. (Eds.), *The Cretaceous System in the Makarov Area, Southern Sakhalin, Russian Far East*. National Science Museum Monographs 31, 1–24.
- Shimura, T., Komatsu, M., Iiyama, J.T., 1992. Genesis of the lower crustal garnet-orthopyroxene tonalites (S-type) of the Hidaka Metamorphic Belt, northern Japan. *Transactions of the Royal Society of Edinburgh: Earth Sciences* 83,259-268.

- Streckeisen, A., Le Maitre, R.W., 1979. A chemical approximation to the modal QAPF classification of the igneous rocks. *Neues Jahrbuch für Mineralogie-Abhandlungen* 136, 169–206.
- Sun, S.S., McDonough, W.E., 1989. Chemical and isotopic systematics of oceanic basalts: implications for mantle composition and processes. In: Karthika, A.D., Norry, M.J. (Eds.), *Magmatism in the Ocean Basins*, vol. 42. Geological Society of London Special Publications, pp. 313–345.
- Sylvester, P.J., 1998. Post-collisional strongly peraluminous granites. *Lithos* 45, 29–44.
- Taira, A., 2001. Tectonic evolution of the Japanese island arc system. *Annual Review of Earth and Planetary Sciences* 29, 109–134.
- Takahashi, H., Kasahara, M., Kimata, F., Miura, S., Heki, K., Seno, T., Kato, T., Vasilenko, N., Ivashchenko, A., Bahtiarov, V., Levin, V., Gordeev, E., Korchagin, F., Gerasimenko, M., 1999. Velocity field of around the Sea of Okhotsk and Sea of Japan regions determined from a new continuous GPS network data. *Geophysical Research Letters* 26, 2533–2536.
- Tang, J., Xu, W., Niu, Y., Wang, F., Ge, W., Sorokin, A.A., Chekryzhov, I.Y., 2016. Geochronology and geochemistry of Late Cretaceous-Paleocene granitoids in the Sikhote-Alin Orogenic Belt: petrogenesis and implications for the oblique subduction of the paleo-Pacific plate. *Lithos* 266–267, 202–212.
- Ueda, H., 2005. Accretion and exhumation structures formed by deeply subducted seamounts in the zircon geochronology, Sr-Nd-Hf isotopic and geochemical analyses Kamuikotan high-pressure/temperature zone, Hokkaido, Japan. *Tectonics* 24, 1–17, TC2007, <http://dx.doi.org/10.1029/2004TC001690>

- Ueda, H., 2016. Hokkaido. from: MORENO, T., WALLIS, S., KOJIMA, T. & GIBBONS, W. (eds). *The Geology of Japan*. Geological Society, London, 201–221.
- Weaver, R., Roberts, A.P., Flecker, R., Macdonald, D.I.M., Fot'yanova, L.M., 2003. Geodynamic implications of paleomagnetic data from Tertiary sediments in Sakhalin, Russia (NW Pacific). *Journal of Geophysical Research* 108, 2066, doi: 10.1029/2001JB001226.
- Weaver, R., Roberts, A.P., Flecker, R., Macdonald, D.I.M., 2004. Tertiary geodynamics of Sakhalin (NW Pacific) from anisotropy of magnetic susceptibility fabrics and paleomagnetic data. *Tectonophysics* 379, 25-42.
- Whalen, J.B., Currie, K.L., Chappel, B.W., 1987. A-type granites: geochemical characteristics, discrimination and petrogenesis. *Contributions to Mineralogy and Petrology* 95(4), 407-419.
- Worrall, D.M., Kruglyak, V., Kunst, F., Kuznetsov, V., 1996. Tertiary tectonics of the Sea of Okhotsk, Russia: Far-field effects of the India-Eurasia collision. *Tectonics* 15(4), 813-826.
- Wu, J.T.J., Jahn, B., Nechaev, V., Chashchin, A., Popov, V., Yokoyama, K., Tsutsumi, Y., 2017. Geochemical characteristics and petrogenesis of adakites in the Sikhote-Alin area, Russian Far East. *Journal of Asian Earth Sciences* 145, 512–529.
- Zhao, P., Jahn, B., Xu, B., Liao, W., Wang, Y., 2016. Geochemistry, geochronology and zircon Hf isotopic study of peralkaline-alkaline intrusions along the northern margin of the North China Craton and its tectonic implication for the southeastern Central Asian Orogenic Belt. *Lithos* 261, 92–108.

- Zhao, P., Jahn, B-M., Xu, B., 2017a. Elemental and Sr-Nd isotopic geochemistry of Cretaceous to Early Paleogene granites and volcanic rocks in the Sikhote-Alin Orogenic Belt (Russian Far East): implications for the regional tectonic evolution. *Journal of Asian Earth Sciences* 146, 383–401.
- Zhao, P., Li, J-J., Alexandrov, I., Ivin, V., Jahn, B-M., 2017b. Involvement of old crustal materials during formation of the Sakhalin Island (Russian Far East) and its paleogeographic implication: Constraints from detrital zircon ages of modern river sand and Miocene sandstone. *Journal of Asian Earth Sciences* 146, 412–430.
- Zhao, P., Alexandrov, I., Jahn, B-M., Ivin, V., 2018. Timing of Okhotsk Sea Plate collision with Eurasia Plate: Zircon U-Pb age constrains from the Sakhalin Island, Russian Far East. *Journal of Geophysical Research: Solid Earth*, doi: 10.1029/2018JB015800.
- Zharov, A.E., 2005. South Sakhalin tectonics and geodynamics: A model for the Cretaceous-Paleogene accretion of the East Asian continental margin. *Russian Journal of Earth Sciences* 7, ES5002, doi:10.2205/2005ES000190
- Zyabrev, S.V., 2011. Stratigraphy and structure of the central East Sakhalin accretionary wedge (Eastern Russia). *Russian Journal of Pacific Geology* 5, 313-35.
- Zyabrev, S.V., 2015. Seamount subduction likely provoked prolific mass wasting on the slope in the central part of the East Sakhalin accretionary wedge, eastern Russia. *Island Arc* 24, 282–287.

Table and Figure captions

Table 1. Complied zircon U-Pb dating result of the late Cretaceous-early Paleogene granitic and volcanic rocks in the Sikhote-Alin, Sakhalin and Hokkaido areas.

Table 2. Brief description of analyzed granitic samples of the Langeri and Val'za plutons in the central Sakhalin Island.

Table 3. Whole-rock chemical compositions of granitic samples of the Langeri and Val'za plutons.

Table 4. Sr-Nd isotopic data of granitic samples of the Langeri and Val'za plutons.

Figure 1. (a) Plate configuration and location of the Sakhalin Island in NE Asia (modified after Seno et al., 1996 and Rodnikov et al., 2014). (b) Principal tectonostratigraphic terranes in NE Asia, including Russian Far East, Sakhalin and Hokkaido Islands (after Golozoubov, 2006; Zharov, 2005; Abrajevitch et al., 2012). Ages of Eocene granites are from Kemp et al., 2007; Jahn et al., 2014; Liao et al., 2018.

Figure 2. (a) Geological map of the southern and central Sakhalin Island, with locations of Langeri and Val'za plutons (Compiled from Ivashchenko et al., 1997; Weaver et al., 2003). (b) Detailed geological map showing location of Langeri and Val'za plutons that intruded into the Verhnelangeri metamorphic complex (modified from 1:200 000 geological map; Galversen et al., 2009). Samples numbers and locations are marked.

Figure 3. Field outcrop and photomicrographs of granite and granodiorite, showing the mineral phases and textures. Q: Quartz; Kfs: K-feldspar; Pl: Plagioclase; Bt: Biotite; Hbl: Hornblende.

Figure 4. Cathodoluminescence (CL) images of representative zircon grains. Circles represent dating points and diameters of circles are 30 μm .

Figure 5. Zircon U–Pb concordia diagrams for granitic samples from the Langeri and Val'za plutons.

Figure 6. Geochemical classification diagrams for granitic rocks of the Langeri and Val'za plutons. (a) SiO_2 versus total alkali ($\text{Na}_2\text{O}+\text{K}_2\text{O}$) content diagram (after Middlemost, 1994); (b) The normative Q'-ANOR plot of Streckeisen and Le Maitre (1979); (c) A/NK vs. A/CNK diagram (after Maniar and Piccoli, 1989); (d) SiO_2 versus $\text{Na}_2\text{O}+\text{K}_2\text{O}-\text{CaO}$ diagram (after Frost et al., 2001). Data source: Cretaceous-Paleogene granites from Sikhote-Alin (Jahn et al., 2015; Zhao et al., 2017a); Eocene granite from southern Sakhalin Island (Liao et al., 2018); Eocene-Miocene granite from Hokkaido (Jahn et al., 2014)

Figure 7. Chondrite-normalized rare earth element patterns and Primitive mantle-normalized trace element spider diagrams of granitic rocks of the Langeri and Val'za plutons (Chondrite and Primitive mantle values are from Sun and McDonough, 1989).

Figure 8. (a) The FeO/MgO vs (Zr + Nb + Ce + Y) plot of Whalen et al. (1987), showing granitic samples from Langeri and Val'za plutons are unfractionated granites. Data sources are the same as Figure 6.

Figure 9. Initial $^{87}\text{Sr}/^{86}\text{Sr}$ versus $\epsilon\text{Nd(t)}$ diagram (a) for granitic samples of the Langeri and Val'za plutons. Data of granites in the Sikhote-Alin are from Jahn et al., 2015 and Valui and Moskalenko, 2010. Data of volcanic rocks in the Sikhote-Alin are from Zhao et al., 2017a. Data of Cenozoic granite and volcanic rocks in the Hokkaido Island are from Jahn et al., 2014. Data of Eocene granite in southern Sakhalin Island are from Liao et al., 2018.

Figure 10. Plots of (a) Rb/Sr versus Rb/Ba (Sylvester, 1998), (b) Molar $\text{Al}_2\text{O}_3/(\text{MgO} + \text{FeO}^T)$ versus molar $\text{CaO}/(\text{MgO} + \text{FeO}^T)$ (Altherr et al., 2000), (c) $\text{Al}_2\text{O}_3/(\text{FeO}+\text{MgO}+\text{TiO}_2)$ versus $\text{Al}_2\text{O}_3+\text{FeO}+\text{MgO}+\text{TiO}_2$ and (d) $(\text{Na}_2\text{O}+\text{K}_2\text{O})/(\text{FeO}+\text{MgO}+\text{TiO}_2)$ versus $\text{Na}_2\text{O}+\text{K}_2\text{O}+\text{FeO}+\text{MgO}+\text{TiO}_2$ diagrams (partial melting of felsic pelites, metagreywackes, and amphibolites obtained in experimental studies; Patiño Douce 1999), (e) Ba versus Sr and (f) Rb/Sr versus Sr of granitic samples from the Langeri and Val'za plutons.

Table 1. Complied zircon U-Pb dating result of Late Cretaceous-Early Paleogene granitic and volcanic rocks in the Sikhote-Alin, Sakhalin and Hokkaido areas.

sample No.	rock type	pluton name	location	age	method	reference
8-881/2	granodiorite	Wrangel	Sikhote-Alin	93±1	LA-ICPMS	Jahn et al., 2015
8-02-1	monzogranite	Ovseenko Cap	Sikhote-Alin	68±1	LA-ICPMS	Jahn et al., 2015
GV-1583-2	monzogranite	Sadovsky	Sikhote-Alin	86±1	LA-ICPMS	Jahn et al., 2015
GV-722	granite	Shumnensky	Sikhote-Alin	75±1	LA-ICPMS	Jahn et al., 2015
GV-1774	granite	Ladoshinsky	Sikhote-Alin	88±1	LA-ICPMS	Jahn et al., 2015
B984	granite	Valentinovsky	Sikhote-Alin	78±1	LA-ICPMS	Jahn et al., 2015
B919b	granite	Valentinovsky	Sikhote-Alin	81±1	LA-ICPMS	Jahn et al., 2015
B621	diorite	Olginsky	Sikhote-Alin	71±1	LA-ICPMS	Jahn et al., 2015
B783M	granodiorite	Olginsky	Sikhote-Alin	78±1	LA-ICPMS	Jahn et al., 2015
B574	granite	Olginsky	Sikhote-Alin	83±1	LA-ICPMS	Jahn et al., 2015
B448	granodiorite	Vladimirsky	Sikhote-Alin	64±1	LA-ICPMS	Jahn et al., 2015
B456	granite	Vladimirsky	Sikhote-Alin	71±1	LA-ICPMS	Jahn et al., 2015
B719	granite	Vladimirsky	Sikhote-Alin	71±1	LA-ICPMS	Jahn et al., 2015
B300	diorite	Oprichninsky	Sikhote-Alin	56±1	LA-ICPMS	Jahn et al., 2015
B301a	granite	Oprichninsky	Sikhote-Alin	57±1	LA-ICPMS	Jahn et al., 2015
14RF34-1	monzogranite	Olga Town	Sikhote-Alin	56±1	LA-ICPMS	Tang et al., 2016
14RF35-1	monzogranite	Valentin	Sikhote-Alin	83±1	LA-ICPMS	Tang et al., 2016
14RF37-1	syenogranite	Benevskoye	Sikhote-Alin	91±1	LA-ICPMS	Tang et al., 2016
14RF37-6	syenogranite	Benevskoye	Sikhote-Alin	92±1	LA-ICPMS	Tang et al., 2016
SAL-55	granite		Sikhote-Alin	76±1	LA-ICPMS	Zhao et al., 2017a
SAL-15	andesite		Sikhote-Alin	74±1	LA-ICPMS	Zhao et al., 2017a
SAL-16	rhyolite		Sikhote-Alin	73±1	LA-ICPMS	Zhao et al., 2017a
SAL-42	rhyolite		Sikhote-Alin	67±1	LA-ICPMS	Zhao et al., 2017a
SAL-52	rhyolite		Sikhote-Alin	79±1	LA-ICPMS	Zhao et al., 2017a
SAL-56	rhyolite		Sikhote-Alin	80±1	LA-ICPMS	Zhao et al., 2017a
SAL-57	rhyolite		Sikhote-Alin	57±1	LA-ICPMS	Zhao et al., 2017a
SAL-61	andesite		Sikhote-Alin	64±1	LA-ICPMS	Zhao et al., 2017a
SAL-62	rhyolite		Sikhote-Alin	67±1	LA-ICPMS	Zhao et al., 2017a
Cha2356	dacite	Frunze	Sikhote-Alin	41±2	LA-ICPMS	Wu et al., 2017
Cha2357	dacite	Frunze	Sikhote-Alin	43±1	LA-ICPMS	Wu et al., 2017
Cha2320/1	dacite	Shkol'naya	Sikhote-Alin	45±2	LA-ICPMS	Wu et al., 2017
Cha2231/2	dacite	Ilistaya	Sikhote-Alin	45±2	LA-ICPMS	Wu et al., 2017
SK14-02	granite	Okhotsk	Sakhalin	43±1	LA-ICPMS	Liao et al., 2018
SK14-03	granite	Okhotsk	Sakhalin	44±1	LA-ICPMS	Liao et al., 2018
SK14-04	granite	Okhotsk	Sakhalin	43±1	LA-ICPMS	Liao et al., 2018

SK14-05	granite	Okhotsk	Sakhalin	43±1	LA-ICPMS	Liao et al., 2018
SK14-06b	granite	Okhotsk	Sakhalin	42±1	LA-ICPMS	Liao et al., 2018
SK14-7	granodiorite	Okhotsk	Sakhalin	43±1	LA-ICPMS	Liao et al., 2018
SK14-15	granite	Okhotsk	Sakhalin	44±1	LA-ICPMS	Liao et al., 2018
SK14-10	rhyolite dike	Okhotsk	Sakhalin	43±1	LA-ICPMS	Liao et al., 2018
SK14-12	rhyolite dike	Okhotsk	Sakhalin	43±1	LA-ICPMS	Liao et al., 2018
SK14-14	rhyolite dike	Okhotsk	Sakhalin	44±1	LA-ICPMS	Liao et al., 2018
SK15-01	aplite	Aniva	Sakhalin	41±1	LA-ICPMS	Liao et al., 2018
SK15-02	granodiorite	Aniva	Sakhalin	41±1	LA-ICPMS	Liao et al., 2018
SK15-03	biotite granite	Aniva	Sakhalin	40±1	LA-ICPMS	Liao et al., 2018
SK15-04	granodiorite	Aniva	Sakhalin	41±1	LA-ICPMS	Liao et al., 2018
SK15-06	granodiorite	Aniva	Sakhalin	41±1	LA-ICPMS	Liao et al., 2018
SK15-07	granodiorite	Aniva	Sakhalin	41±1	LA-ICPMS	Liao et al., 2018
SK15-08	granite	Aniva	Sakhalin	40±1	LA-ICPMS	Liao et al., 2018
SK15-09	granodiorite	Aniva	Sakhalin	41±1	LA-ICPMS	Liao et al., 2018
UTT-2	monzogranite	Uttsu-dake	Hokkaido	45±1	LA-ICPMS	Jahn et al., 2014
AB-1	monzogranite	Aibetsu	Hokkaido	45±1	LA-ICPMS	Jahn et al., 2014
UK-1	monzogranite	Ukishima	Hokkaido	45±1	LA-ICPMS	Jahn et al., 2014
ST-1	monzogranite	Shirataki	Hokkaido	37±1	LA-ICPMS	Jahn et al., 2014
	granite+tonalite	Hidaka	Hokkaido	37±1	LA-ICPMS	Kemp et al., 2007

Table 2 Brief description of analyzed granitic rocks of the Langeri and Val'za plutons in the central Sakhalin Island.

Samples No.	Pluton	Rock type	Sample locality (GPS)	Petrographic texture	Mineral assemblage ^a
SK15-20	Langeri	Granodiorite	N50°1'42.2", E143°5'1.2"	porphyritic texture with plagioclase and hornblende phenocryst	Pl (40%), Q (25%), Hbl (15%), Kfs (10%), Bt (5%)
SK 15-21	Langeri	Granodiorite	N50°1'39.8", E143°4'53.2"	porphyritic texture with plagioclase and hornblende phenocryst	Pl (40%), Q (25%), Hbl (15%), Kfs (10%), Bt (5%)
SK 15-22	Langeri	Monzogranite	N50°1'39.1", E143°4'53.3"	Coarse-grained granitic texture	Kfs (35%), Q (25%), Pl (20%), Bt (10%)
SK 15-23 ^b	Langeri	Monzogranite	N50°2'0.2", E143°4'38.2"	Fine-grained granitic texture	Kfs (35%), Q (25%), Pl (20%), Bt (10%)
SK 15-24	Langeri	Monzogranite	N50°2'0.2", E143°4'38.2"	Coarse-grained granitic texture	Kfs (35%), Q (25%), Pl (20%), Bt (10%)
SK 15-25	Langeri	Granodiorite	N50°2'11.8", E143°4'40.3"	Coarse-grained granitic texture	Pl (40%), Q (25%), Hbl (15%), Kfs (10%), Bt (5%)
SK 15-27 ^b	Langeri	Monzogranite	N50°2'15.9", E143°4'22.5"	Coarse-grained granitic texture	Kfs (35%), Q (25%), Pl (20%), Bt (10%)
SK 15-32	Val'za	Granodiorite	N50°13'49.2", E143°01'55.8"	Fine-grained granitic texture	Pl (40%), Q (25%), Hbl (15%), Kfs (10%), Bt (5%)
SK 15-33 ^b	Val'za	Monzogranite	N50°13'52.8", E143°01'44.1"	Coarse-grained granitic texture	Kfs (35%), Q (25%), Pl (20%), Bt (10%)
SK 15-34	Val'za	Monzogranite	N50°13'51.6", E143°01'42.1"	Coarse-grained granitic texture	Kfs (35%), Q (25%), Pl (20%), Bt (10%)
SK 15-35	Val'za	Granodiorite	N50°15'03.9" E142°59'04.2"	Coarse-grained granitic texture	Pl (40%), Q (25%), Hbl (15%), Kfs (10%), Bt

					(5%)
SK 15-36 ^b	Val'za	Granodiorite	N50°15'08.4", E142°59'05.6"	porphyritic texture with plagioclase and hornblende phenocryst	Pl (40%), Q (25%), Hbl (15%), Kfs (10%), Bt (5%)
SK 15-37	Val'za	Granodiorite	N50°15'08.3" E142°59'05.7"	porphyritic texture with plagioclase and hornblende phenocryst	Pl (40%), Q (25%), Hbl (15%), Kfs (10%), Bt (5%)
SK 15-38	Val'za	Granodiorite	N50°15'04.1" E142°58'27.7"	porphyritic texture with plagioclase and hornblende phenocryst	Pl (40%), Q (25%), Hbl (15%), Kfs (10%), Bt (5%)
SK 15-39	Val'za	Tonalite	N50°15'01.9" E142°58'08.9"	Coarse-grained granitic texture	Pl (50%), Q (25%), Hbl (15%), Bt (5%)
SK 15-40	Val'za	Monzogranite	N50°12'52.8" E142°58'29.8.9"	Coarse-grained granitic texture	Kfs (35%), Q (25%), Pl (20%), Bt (10%)

^a Mineral name abbreviations: Q = quartz, Pl = plagioclase, Kfs = alkali feldspar, Hbl = hornblende, Bt = biotite.

^b Zircon ages and geochemical data of these four samples will be reported in another paper (Zhao et al., 2018).

Table 3 Whole-rock chemical compositions of granitic rock samples of the Langeri and Val'za plutons

Pluton		Langeri						Val'za										
Sample name		SK1 5-20	SK1 5-21	SK1 5-22	SK1 5-23	SK1 5-24	SK1 5-25	SK1 5-27	SK1 5-32	SK1 5-33	SK1 5-34	SK1 5-35	SK1 5-36	SK1 5-37	SK1 5-38	SK1 15-39	SK1 5-40	
Rock type		gran odio rite	gran odio rite	mon zogr anite	gran odio rite	mon zogr anite	mon zogr anite	gran odio rite	gran odio rite	gran odio rite	gran odio rite	ton alite	mon zogr anite					
SiO ₂		68.04	65.66	76.20	72.24	73.19	69.19	75.36	68.70	73.88	74.52	69.33	69.16	68.55	69.53	63.79	71.34	
TiO ₂		0.41	0.44	0.15	0.36	0.24	0.52	0.18	0.39	0.19	0.18	0.39	0.41	0.41	0.37	0.46	0.28	
Al ₂ O ₃		15.84	17.41	13.23	14.99	14.38	15.53	13.62	16.21	14.76	14.04	15.26	15.64	15.74	15.54	16.55	15.15	
Fe ₂ O ₃		2.86	3.28	1.10	2.02	1.77	3.20	1.38	2.90	1.44	1.38	2.73	2.83	2.95	2.58	3.76	2.00	
CaO		1.79	3.02	0.79	1.60	1.48	2.69	1.35	2.99	2.00	1.56	1.70	2.56	2.58	2.78	4.73	2.11	
MgO		1.61	1.96	0.48	0.71	0.85	1.36	0.64	1.43	0.69	0.62	1.07	1.11	1.67	1.20	3.46	0.82	
MnO		0.05	0.06	0.03	0.04	0.04	0.07	0.03	0.05	0.04	0.04	0.07	0.07	0.07	0.06	0.06	0.07	0.05
Na ₂ O		4.14	3.51	3.58	3.72	3.74	3.76	3.54	4.17	3.94	3.69	3.84	3.58	4.06	3.96	3.54	3.87	
K ₂ O		2.40	2.40	3.99	3.75	3.36	2.89	3.47	1.96	2.76	3.31	3.34	2.85	2.50	2.54	1.26	3.09	
P ₂ O ₅		0.11	0.11	0.03	0.08	0.08	0.15	0.04	0.11	0.06	0.05	0.14	0.14	0.10	0.11	0.11	0.09	
LOI		3.02	2.74	0.55	0.86	0.96	0.87	0.51	1.30	0.72	0.70	2.43	1.53	1.60	1.48	2.15	0.79	
A/NK		1.67	2.07	1.28	1.46	1.46	1.65	1.41	1.79	1.55	1.44	1.52	1.73	1.67	1.66	2.29	1.55	
A/CNK		1.25	1.25	1.13	1.14	1.14	1.09	1.12	1.12	1.12	1.12	1.16	1.14	1.11	1.08	1.04	1.11	
TOTAL		100.27	100.58	100.13	100.36	100.09	100.23	100.12	100.20	100.48	100.09	100.29	99.90	100.22	100.16	99.89	99.59	
Sc		13	8	20	16	16	24	18	15	15	16	14	14	8	15	13	21	
V		48	58	9	21	19	47	12	39	13	12	32	34	39	30	65	28	
Cr		60	107	7	101	20	22	36	38	9	56	41	43	42	40	105	61	
Co		5.7	9.7	1.1	3.8	3.5	6.3	2.8	5.5	2.6	2.4	4.9	5.4	7.3	5.4	13	4.1	
Ni		51	53	37	142	17	6.7	27	23	14	16	25	28	35	35	52	24	
Ga		18	24	13	24	19	19	12	19	14	12	16	17	17	15	17	34	
Rb		103	89	172	158	131	124	140	80	105	122	137	88	83	97	34	123	
Sr		297	374	50	141	138	192	117	388	198	156	298	299	290	291	411	214	
Y		15.6	19.9	34.5	22.2	24.1	23.8	20.6	15.8	16.9	16.1	21.3	20.6	19.8	18.4	164	17.4	
Zr		132	147	87	200	105	168	80	120	91	103	142	142	139	135	122	118	
Nb		6.0	7.8	7.0	11.3	6.9	10.1	6.5	5.4	6.6	6.3	9.8	9.7	7.2	7.7	5.4	7.3	
Cs		7.3	6.3	7.6	10.6	8.5	10.9	8.8	10.4	8.0	8.1	6.8	7.3	2.5	6.5	3.2	9.6	
Ba		474	554	313	619	448	435	419	626	451	612	758	661	518	623	429	620	
La		14.8	19.9	22.8	22.2	23.4	23.0	20.7	13.8	15.1	21.8	21.9	20.5	19.2	16.2	144	19.1	
Ce		34.6	41.2	51.2	47.9	48.9	50.9	43.7	28.3	30.6	44.4	43.9	41.7	40.3	33.9	309	39.1	
Pr		3.8	4.8	6.0	5.5	5.7	6.0	4.9	3.4	3.4	4.9	5.3	5.0	4.7	4.0	3.7	4.5	
Nd		15.1	18.3	22.3	21.0	21.0	23.6	17.8	13.1	12.4	17.9	20.3	19.2	18.1	15.2	146	16.7	
Sm		3.3	3.8	5.1	4.3	4.4	5.1	3.6	2.8	2.7	3.5	4.3	4.1	3.8	3.3	3.1	3.5	

Eu	0.6	0.9	0.2	0.5	0.4	0.7	0.4		0.7	0.5	0.5	0.8	0.8	0.7	0.7	0.7	0.6
Gd	2.9	3.6	4.9	3.8	4.0	4.6	3.2		2.7	2.6	2.9	3.9	3.7	3.5	3.2	3.0	3.1
Tb	0.47	0.56	0.83	0.62	0.64	0.71	0.53		0.44	0.44	0.43	0.62	0.59	0.54	0.51	0.4 ₆	0.50
Dy	2.7	3.4	5.2	3.7	3.8	4.1	3.2		2.6	2.6	2.5	3.6	3.5	3.3	3.1	2.7	2.9
Ho	0.52	0.67	1.08	0.73	0.77	0.81	0.66		0.52	0.55	0.51	0.70	0.68	0.64	0.61	0.5 ₅	0.58
Er	1.5	1.9	3.3	2.1	2.2	2.3	2.0		1.5	1.6	1.5	2.0	1.9	1.9	1.7	1.6	1.6
Tm	0.22	0.30	0.55	0.33	0.35	0.34	0.31		0.22	0.25	0.25	0.30	0.30	0.29	0.27	0.2 ₄	0.25
Yb	1.5	2.0	3.7	2.1	2.3	2.2	2.1		1.5	1.7	1.7	1.9	1.9	1.9	1.7	1.5	1.6
Lu	0.22	0.30	0.55	0.32	0.35	0.32	0.32		0.22	0.25	0.28	0.29	0.28	0.28	0.25	0.2 ₃	0.26
Hf	3.4	3.9	3.4	5.0	3.1	4.5	2.8		3.1	2.9	3.0	3.7	3.7	3.7	3.4	3.1	3.2
Ta	0.52	0.65	1.16	0.99	0.75	0.75	1.03		0.42	0.74	0.69	0.85	0.84	0.59	0.67	0.3 ₉	0.64
Pb	14.3	234. ₅	36.8	24.2	26.6	17.2	27.5		7.1	21.5	22.6	16.5	19.3	17.0	16.7	11. ₉	21.9
Th	6.3	7.8	18.1	11.7	12.9	13.6	12.1		4.5	7.2	10.8	8.6	8.3	8.0	6.7	5.5	9.1
U	2.1	2.6	5.3	3.0	2.8	2.5	2.7		1.8	2.9	2.5	2.9	2.8	2.2	2.3	1.6	1.9
δ Eu	0.58	0.77	0.12	0.40	0.31	0.44	0.32		0.82	0.60	0.45	0.59	0.61	0.59	0.63	0.7 ₅	0.55
(La/Yb) _N	7.27	7.32	4.43	7.58	7.39	7.60	6.97		6.83	6.45	9.04	8.31	7.78	7.40	6.80	6.7 ₁	8.41
normative corundum	3.44	3.81	1.64	2.10	2.08	1.66	1.66		2.02	1.77	1.66	2.54	2.33	1.87	1.45	1.0 ₁	1.81

Table 4. Sr-Nd isotopic data of granitic rock samples of the Langeri and Val'za plutons

Sample No.	Rock type	Age (Ma)	[Rb] (ppm)	[Sr] (ppm)	$^{87}\text{Rb}/$ ^{86}Sr	$^{87}\text{Sr}/$ ^{86}Sr	$\pm 2\text{sm}$	I(Sr)	[Sm] (ppm)	[Nd] (ppm)	$^{147}\text{Sm}/$ ^{144}Nd
SK15-20	granodiorite	37	103	297	1.00	0.704790	9	0.70426	3.3	15.1	0.1309
SK15-21	granodiorite	37	89	374	0.69	0.704685	7	0.70432	3.8	18.3	0.1267
SK15-22	monzogranite	37	172	50	9.94	0.709549	7	0.70433	5.1	22.3	0.1377
SK15-23	monzogranite	37	158	141	3.24	0.706051	7	0.70435	4.3	21.0	0.1240
SK15-24	monzogranite	37	131	138	2.74	0.705952	9	0.70451	4.4	21.0	0.1270
SK15-25	granodiorite	37	124	192	1.87	0.705502	8	0.70452	5.1	23.6	0.1299
SK15-27	monzogranite	37	140	117	3.46	0.706188	7	0.70437	3.6	17.8	0.1220
SK15-32	granodiorite	37	80	388	0.59	0.704752	7	0.70444	2.8	13.1	0.1285
SK15-33	monzogranite	37	105	198	1.54	0.705125	7	0.70432	2.7	12.4	0.1307
SK15-34	monzogranite	37	122	156	2.27	0.705506	7	0.70432	3.5	17.9	0.1164
SK15-35	granodiorite	37	137	298	1.32	0.705577	6	0.70488	4.3	20.3	0.1278
SK15-36	granodiorite	37	88	299	0.85	0.704985	7	0.70454	4.1	19.2	0.1280
SK15-37	granodiorite	37	83	290	0.83	0.704926	8	0.70449	3.8	18.1	0.1259
SK15-38	granodiorite	37	97	291	0.97	0.705039	9	0.70453	3.3	15.2	0.1320
SK15-39	tonalite	37	34	411	0.24	0.704510	8	0.70438	3.1	14.6	0.1294
SK15-40	monzogranite	37	123	214	1.66	0.705298	7	0.70443	3.5	16.7	0.1264

$$\varepsilon_{\text{Nd}}(0) = 10^4 * ((^{143}\text{Nd}/^{144}\text{Nd})_{\text{sample}(0)} / (^{143}\text{Nd}/^{144}\text{Nd})_{\text{CHUR}(0)} - 1)$$

$$\varepsilon_{\text{Nd}}(t) = \varepsilon_{\text{Nd}}(0) - Q_{\text{Nd}} * f_s * t \text{ (t in Ga)}$$

$$f_s = f_{\text{Sm/Nd, sample}(0)} = (^{147}\text{Sm}/^{144}\text{Nd})_{\text{sample}(0)} / (^{147}\text{Sm}/^{144}\text{Nd})_{\text{CHUR}(0)} - 1$$

$$T_{\text{DM-1}} = (1/l_{147}) \times \log_e \{ 1 + [(^{143}\text{Nd}/^{144}\text{Nd})_{\text{sample}(0)} - (^{143}\text{Nd}/^{144}\text{Nd})_{\text{DM}}] / [(^{147}\text{Sm}/^{144}\text{Nd})_{\text{sample}} - (^{147}\text{Sm}/^{144}\text{Nd})_{\text{DM}}] \}$$

$$T_{\text{DM-2}} = ((eN_{\text{DM, present}} - eN_{\text{Nd}}(0)_{\text{sample}} + Q \times 0.13 \times (f_s - f_{\text{CC}}))) / (Q \times (f_{\text{DM}} - f_{\text{CC}})) \times 1000$$

$Q = 25.13$ (/Ga) when $^{146}\text{Nd}/^{142}\text{Nd}$ is normalized to 0.63151 (DePaolo, 1988)

$(^{143}\text{Nd}/^{144}\text{Nd})_{\text{CHUR, present}} = 0.512638$ (after Goldstein et al., 1984)

$(^{147}\text{Sm}/^{144}\text{Nd})_{\text{CHUR, present}} = 0.1967$ (after Jacobsen and Wasserburg, 1980)

$\lambda_{147} = 0.00654/\text{Ga}$: decay constant of ^{147}Sm . After Lugmair and Marti (1978)

$(^{143}\text{Nd}/^{144}\text{Nd})_{\text{DM, present}} = 0.51315$

$(^{147}\text{Sm}/^{144}\text{Nd})_{\text{DM, present}} = 0.2137$

$f_{\text{CC}} = f_{\text{Sm/Nd, average continental crust}} = (^{147}\text{Sm}/^{144}\text{Nd})_{\text{aver. cont. crust}} / (^{147}\text{Sm}/^{144}\text{Nd})_{\text{CHUR}} - 1 = -0.4$

Highlights

- Late Eocene (36-38 Ma) granites intruded into the East Sakhalin accretionary complex.
- The Late Eocene granites were generated from anatexis of meta-materials of the accretionary complex.
- Generation of Late Eocene granites are related to the collision of Okhotsk Sea Plate and Eurasia Plate.

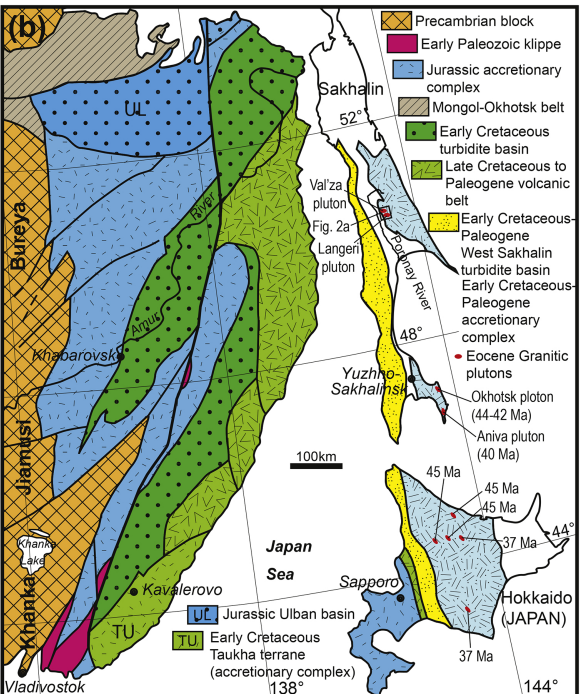
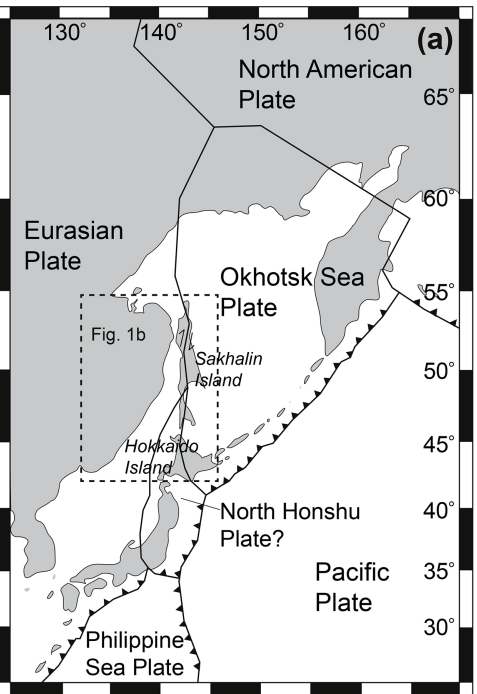


Figure 1

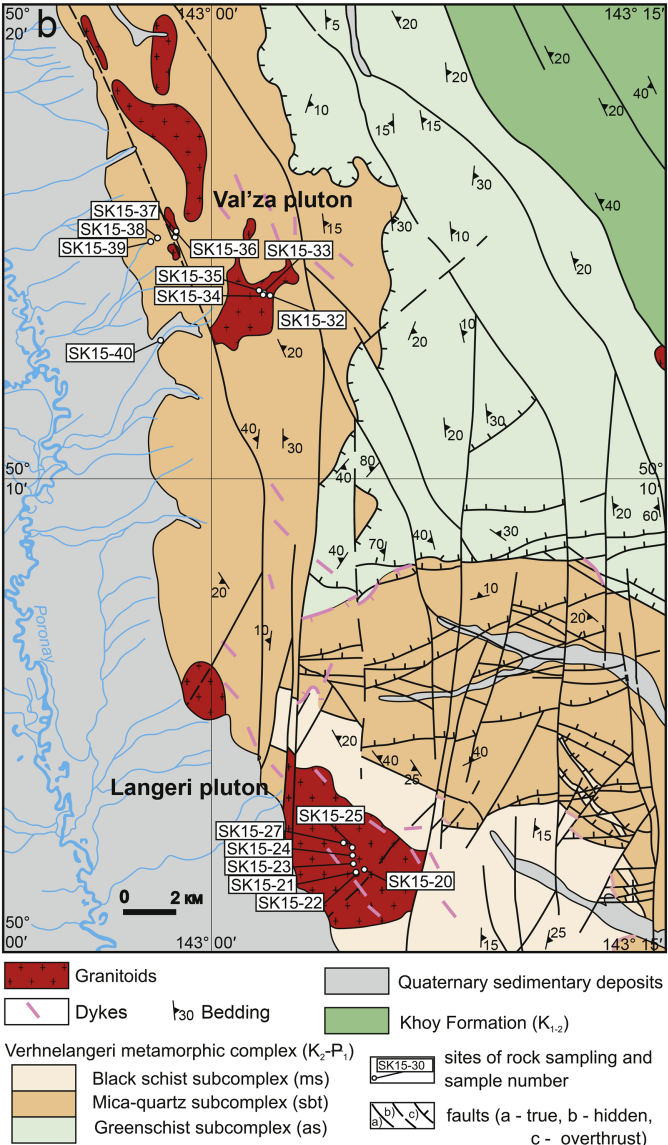
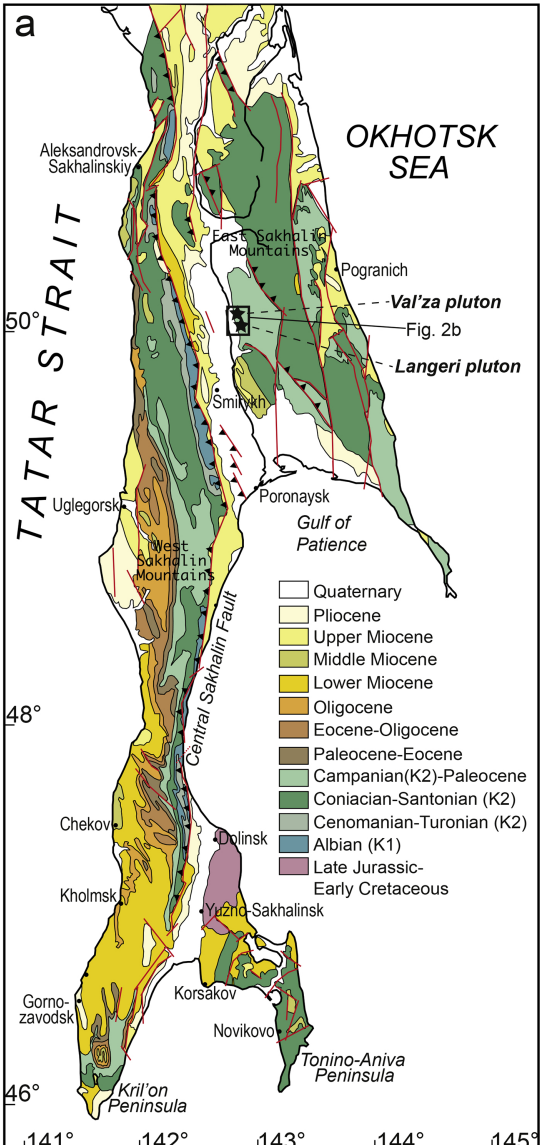


Figure 2

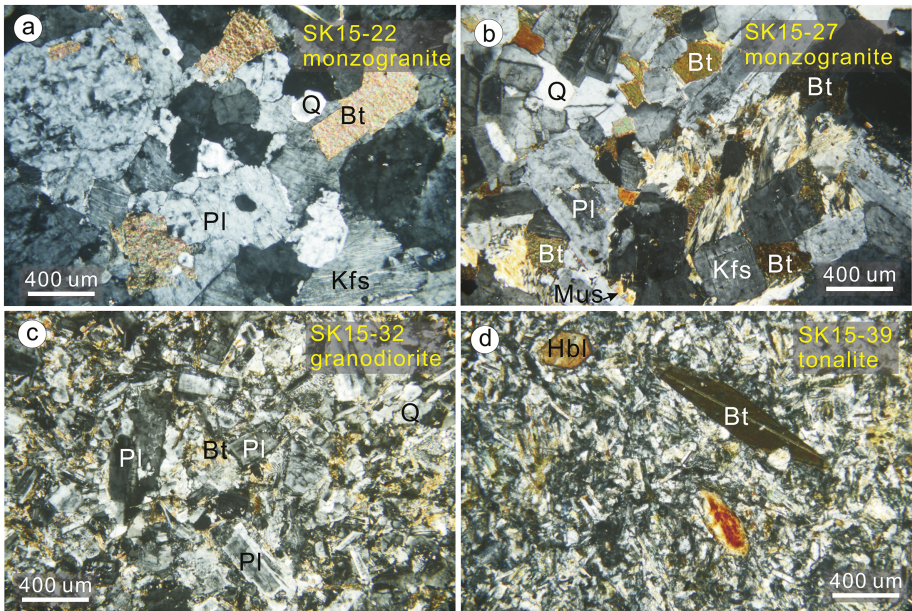


Figure 3

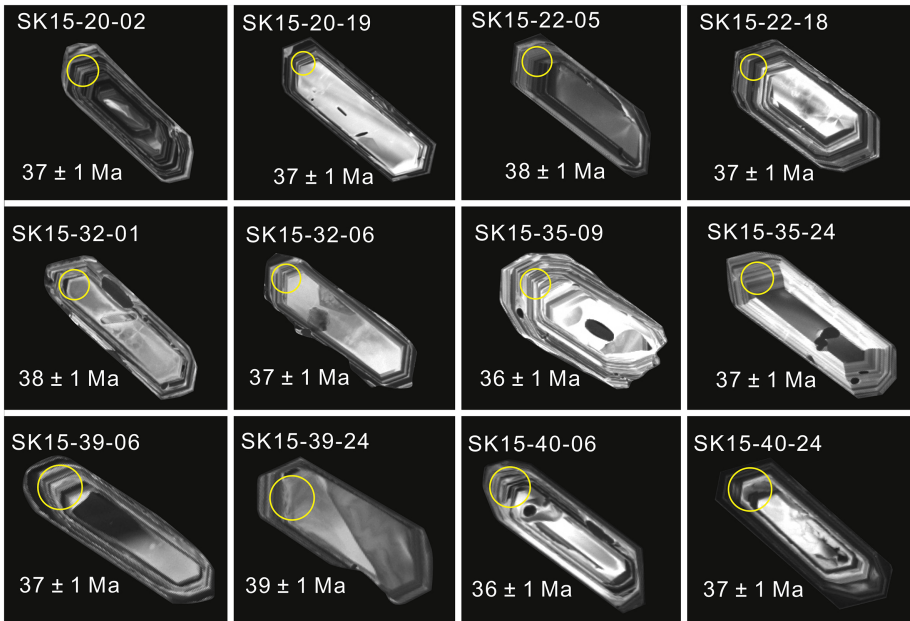


Figure 4

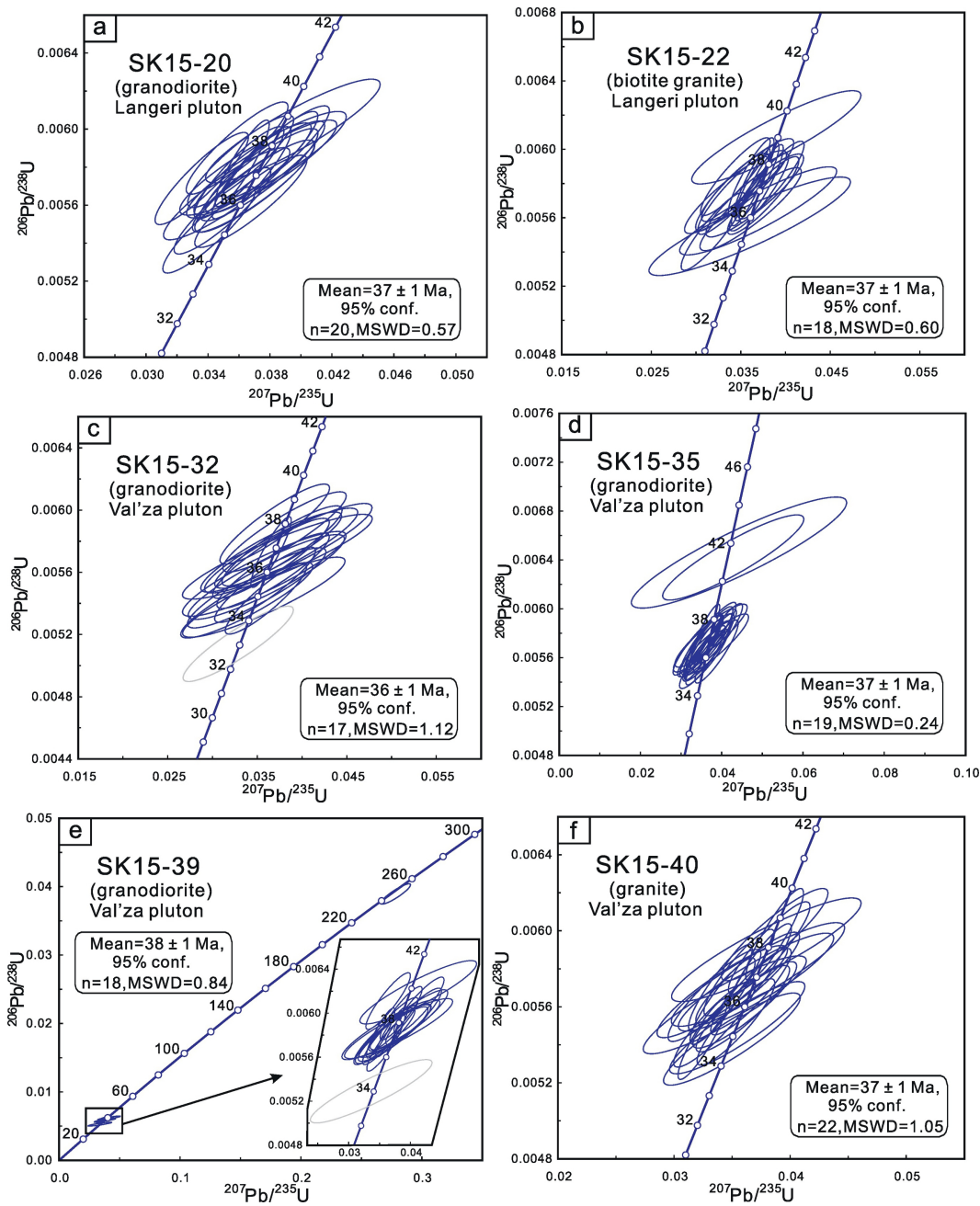


Figure 5

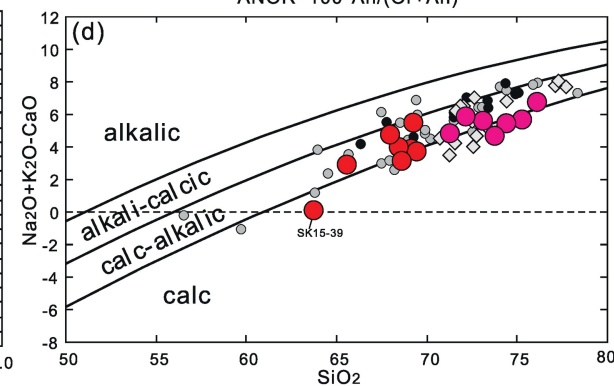
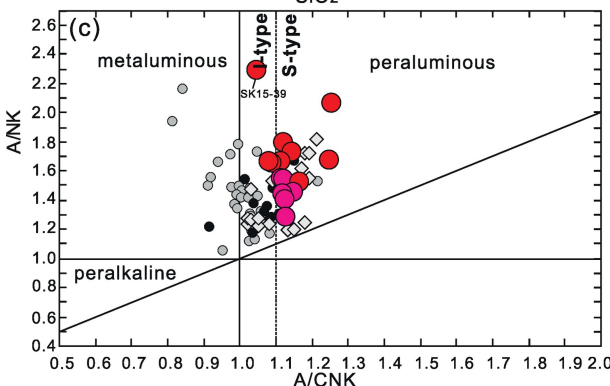
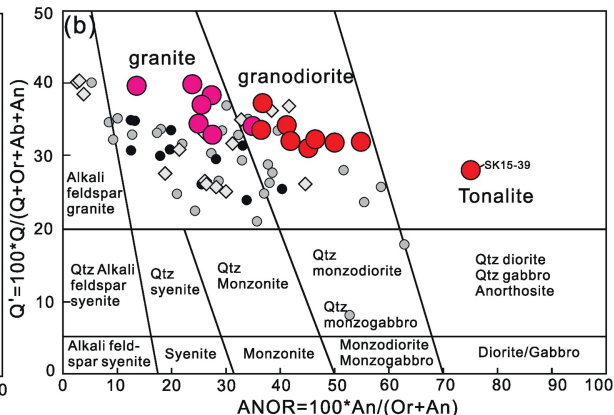
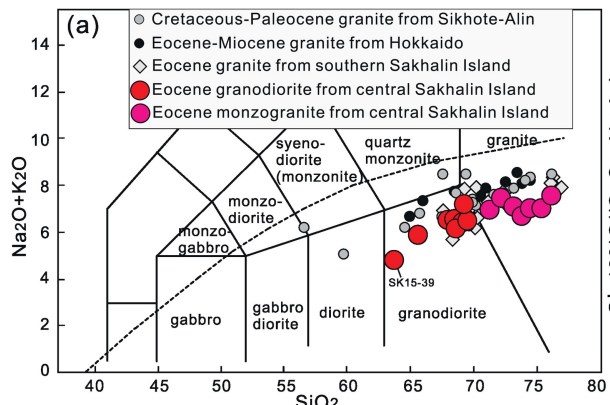


Figure 6

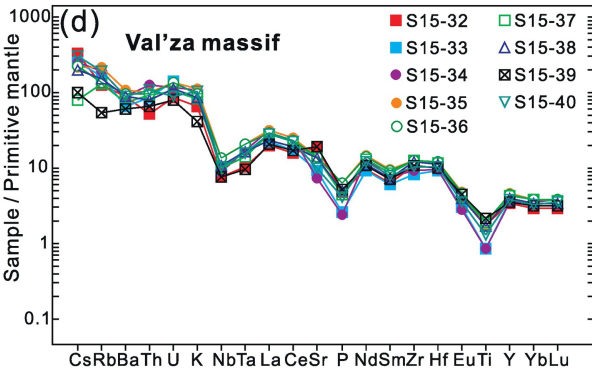
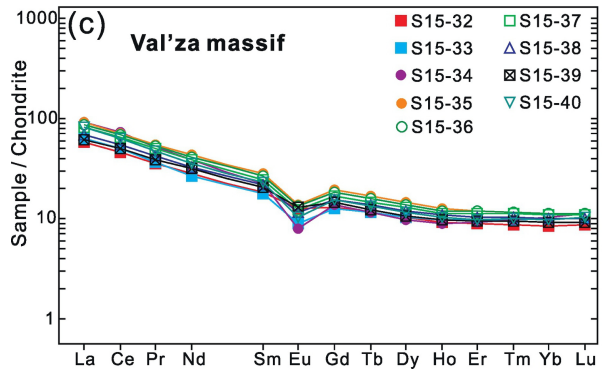
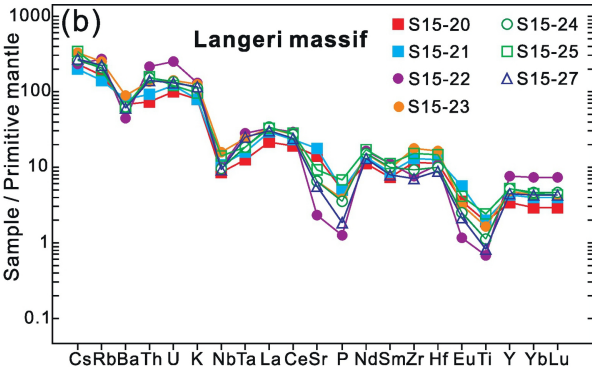
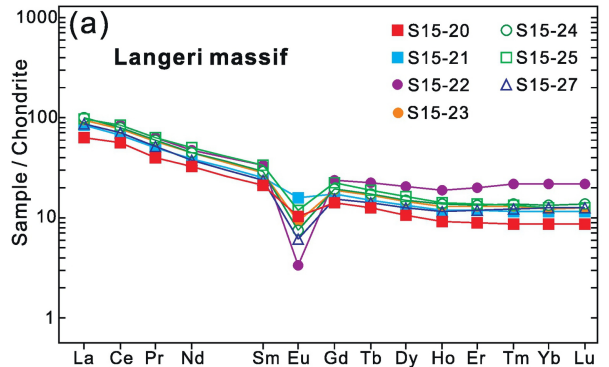


Figure 7

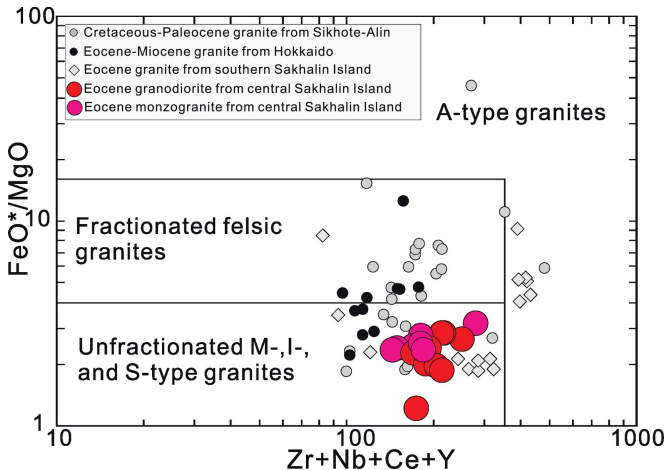


Figure 8

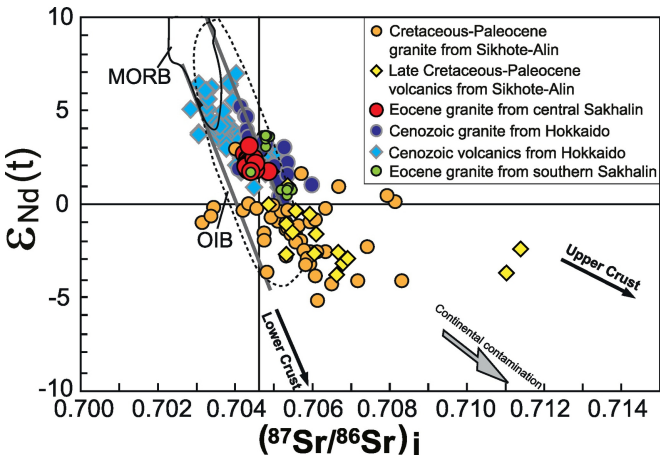


Figure 9

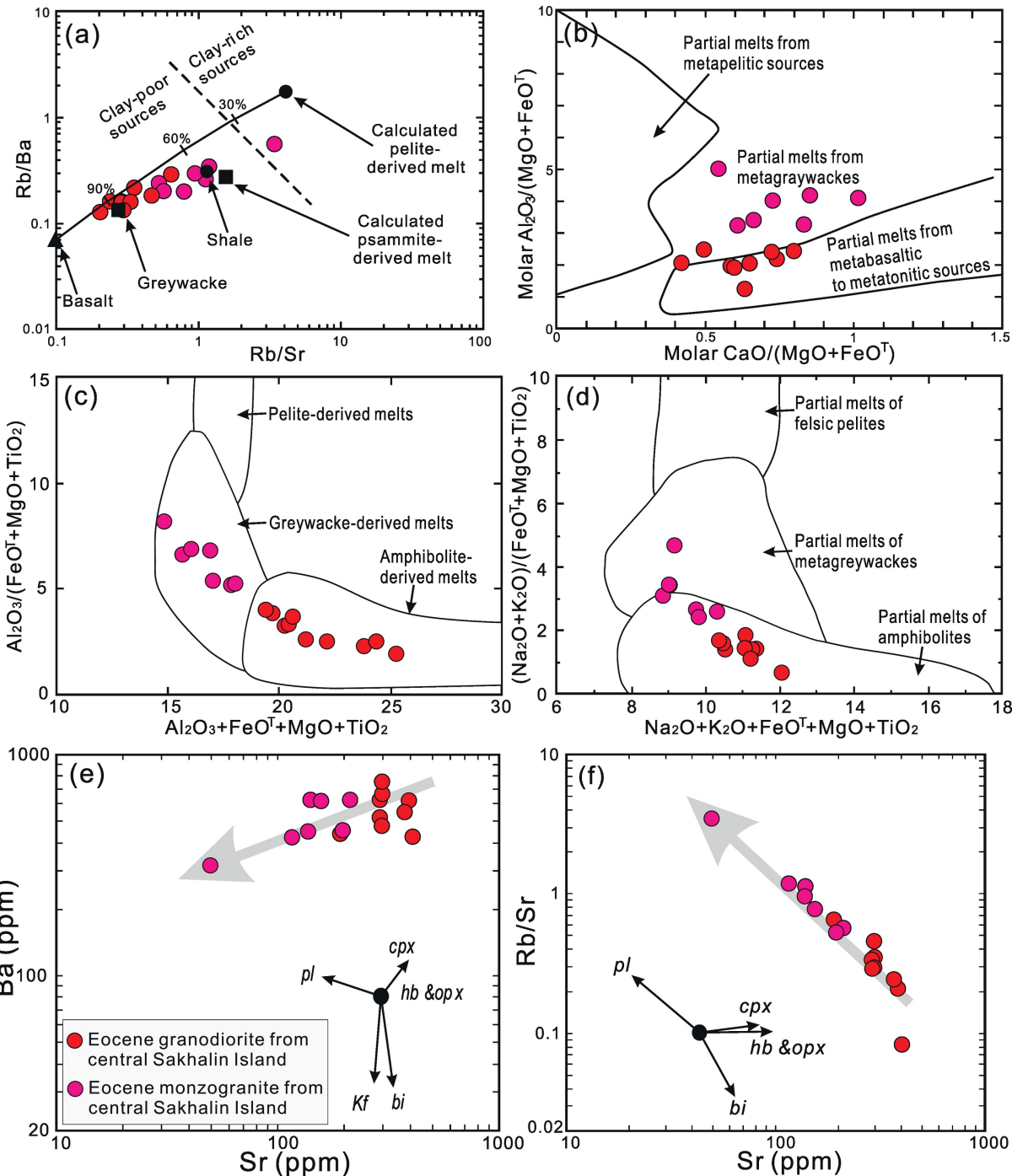


Figure 10